

Sorption of Heavy Metal Contaminants to Particles From Tire Materials

A thesis presented to
the faculty of
the Russ College of Engineering and Technology of Ohio University

In partial fulfillment
of the requirements for the degree
Master of Science

Tawhid Bin Rahmatullah

May 2023

© 2023 Tawhid Bin Rahmatullah. All Rights Reserved.

This thesis titled
Sorpton of Heavy Metal contaminants to Particles From Tire Materials

by
TAWHID BIN RAHMATULLAH

has been approved for
the Department of Civil Engineering
and the Russ College of Engineering and Technology by

Lei Wu
Associate Professor of Environmental Engineering

Maj Mirmirani
Interim Dean, Russ College of Engineering and Technology

Abstract

BIN RAHMATULLAH, TAWHID., M.S., May 2023, Civil Engineering

Sorption of Heavy Metal Contaminants to Particles From Tire Materials

Director of Thesis: Lei Wu

Tire particles (TP) are the largest source of microplastics in nature. However, the adsorption behavior of TP needs to be better understood. TP used in this study were generated from cryo-milling and aged with 30% nitric acid. Single and competitive adsorption isotherm experiments were conducted to investigate the potential of TP as carriers of heavy metals. Langmuir and Freundlich models were used to analyze adsorption data. Competitive adsorption demonstrated a reduction in the adsorption capacity of TP. The preference for lead to copper by TP was explained by the physical and chemical properties of the metals. The adsorption capacity was maximum at the pH range of 6-12 for lead, and for copper, it was pH 10. pH, zeta potential, FT-IR, and XPS results indicated that electrostatic attraction and surface complexation were involved in the heavy metal adsorption on TP.

Dedication

This work is dedicated to my parents.

Acknowledgments

I would like to thank my advisor Dr. Wu for being my mentor, who always believed in me and gave brilliant suggestions. I would also like to thank Dr. Riefler for his words of encouragement and for teaching me to use the AAS machine.

I thank Christian and Farzana Apu for always listening to me and for being my friends. I would also like to thank Binay, Liz, Mamoon for keeping the office fun. To my roommates Hridoy and Shishir – thank you for being partners in late-night silly discussions. I am also grateful to Redoy vai, Saroj, Nazim vai for supporting me.

Finally, I would like to thank my parents, my sister, my brother-in-law, and my nephew Ryan. Thank you for the love, care, and support.

Table of Contents

	Page
Abstract.....	3
Dedication.....	4
Acknowledgments.....	5
List of Tables	8
List of Figures	9
Chapter 1: Project Overview.....	11
1.1 Objectives	14
Chapter 2: Literature Review	15
2.1 Generation of TP.....	15
2.2 Properties of TP	16
2.2.1 Chemical Composition.....	18
2.2.2 Size Distribution	20
2.2.3 Surface Properties	20
2.3 Comparison of TP with Microplastics in Adsorption of Heavy Metals	21
2.4 Heavy Metal Removal by Typical Adsorbents.....	23
2.5 Competitive Adsorption.....	25
2.6 Aging of TP.....	25
2.7 Fate and Transport of Heavy Metals Affected by Adsorption on TP.....	26
2.8 Mechanisms in Heavy Metal Adsorption on TP.....	28
2.9 Influence of Environmental Factors.....	30
2.9.1 Effect of pH on Heavy Metal Adsorption on TP	30
Chapter 3: Methodology	35
3.1 TP Preparation	35
3.2 Preparation of Aged TP	36
3.3 Batch Adsorption Tests.....	37
3.3.1 Single Batch Adsorption Tests.....	38
3.3.2 Competitive Adsorption Tests	41
3.4 Characterization of TP	42
3.4.1 Scanning Electron Microscope (SEM) Imaging	42
3.4.2 Brunauer-Emmet-Teller (BET) Surface Area.....	43

3.4.3 Size Distribution of Aged TP.....	45
3.4.4 Zeta Potential	46
3.4.5 Fourier-Transform Infrared Spectroscopy (FT-IR)	47
3.4.6 X-ray Photoelectron Spectroscopy (XPS)	48
Chapter 4: Results and Discussion.....	50
4.1 Morphology, Surface Area, and Size Distribution.....	50
4.1.1 Discussion	50
4.2 Zeta Potential	51
4.2.1 Discussion	52
4.3 FT-IR Results.....	54
4.3.1 Discussion	56
4.4 XPS Results	57
4.4.1 Discussion	60
4.5 Single Batch Adsorption Results	62
4.5.1 Discussion	64
4.6 Competitive Adsorption Results	67
4.6.1 Discussion	69
4.7 Effect of pH on Adsorption.....	71
4.7.1 Discussion	72
4.8 Effect on Heavy Metal Transport	74
4.9 Insights into the Adsorption Mechanisms.....	75
Chapter 5: Conclusion and future work	76
5.1 Conclusion	76
5.2 Future work.....	79
References.....	81
Appendix A: BET Surface Area Measurement Curves.	94
Appendix B: Screening Test for Adsorbent Dose Used in Isotherm Tests.....	99
Appendix C: Size Distribution of the Finer Portion of the Aged TP.....	109

List of Tables

	Page
Table 1. Comparison among the size, shape, and density of differently generated TP (reproduced from Wagner et al., 2022).....	17
Table 2. Langmuir and Freundlich parameters for lead and copper adsorption on microplastics.	22
Table 3. Langmuir and Freundlich model parameters for lead and copper adsorption on commercial adsorbents and tire-derived activated carbon.....	24
Table 4. Stability constants (logarithms to base 10) for copper (II) and lead (II) at 25°C (reproduced from Rodda et al., 1993).	32
Table 5. Adsorbent dose and heavy metal concentrations used in single batch	39
Table 6. Adsorbent dose and heavy metal concentrations used in competitive batch adsorption tests.....	41
Table 7. Zeta potential and pH of aged TP before and after heavy metal adsorption.	52
Table 8. Langmuir and Freundlich parameters for Pb and Cu adsorption on TP.	63
Table 9. Langmuir & Freundlich parameters for competitive adsorption.	68

List of Figures

	Page
Figure 1. Summary of research objectives and approach.	14
Figure 2. The global TWP generation steadily increased over the years.....	15
Figure 3. A) Basic sections of a tire. B) Percentage of different components of tires (reproduced from <i>What's In a Tire</i> U.S. Tire Manufacturers Association, n.d.).....	19
Figure 4. Sorption mechanism of organic compounds on tire	28
Figure 5. The possible mechanisms involved in heavy metal	29
Figure 6. (A) Lead (reproduced from Powell et al., 2009) and (B) copper (reproduced from Powell et al., 2007) species in aqueous solution as a function of pH.	33
Figure 7. (A) Tire scraps collected from the playground. (B) Small.....	36
Figure 8. (A) Vacuum filtration of TP in the aging process. (B) Centrifuge used to separate TP and adsorbate. (C) Orbital shaker used to mix TP and adsorbate. (D) AAS machine used in measuring equilibrium aqueous phase concentration of adsorbate.....	40
Figure 9. SEM images of (A) untreated (B) aged TP.	50
Figure 10. Zeta potential of aged TP	51
Figure 11. (A-B) FT-IR spectra for Untreated TP, aged TP, lead adsorbed.....	55
Figure 12. Comparison of FT-IR spectra of aged TP before and after heavy metal adsorption.....	57
Figure 13. Pb 4f XPS spectra on aged TP after lead adsorption.....	58
Figure 14. XPS spectra of C1s (A) before and (B) after lead adsorption	59
Figure 15. XPS spectra of O1s (A) before and (B) after lead.....	60
Figure 16. Relative contents of the functional groups	61
Figure 17. Adsorption isotherm of lead for (A) untreated TP and (B) aged TP.	62
Figure 18. Adsorption isotherm of copper for (A) untreated TP and (B) aged TP.....	64
Figure 19. (A) Competitive adsorption isotherm for lead with aged TP. (B) Comparison of single and competitive adsorption isotherm for lead with aged TP.	68
Figure 20. (A) Competitive adsorption isotherm for copper with aged TP.	69
Figure 21. (A) Comparison of maximum adsorption capacity (Q_m) from the Langmuir model for single and competitive adsorption isotherms for lead and copper.	70
Figure 22. Effect of pH on (A) Pb^{2+} and (B) Cu^{2+} adsorption on aged TP at initial concentration 5mg/L.	71
Figure 23. Effect of pH on (A) Pb^{2+} and (B) Cu^{2+} removal efficiency of aged TP at initial concentration 5mg/L.	72

Figure 24.(A) N ₂ adsorption-desorption isotherm and (B) correlation coefficient curve in measurement of BET surface area of untreated TP.	94
Figure 25. Summary report from Surface BET measurement for untreated TP.	95
Figure 26.BET surface area report from Surface BET	95
Figure 27. t-plot report from BET surface area measurement	96
Figure 28. Summary report from surface BET	96
Figure 29. BET Surface area report from BET measurement of aged TP.	97
Figure 30. Pore distribution report from BET surface area measurements of aged TP....	97
Figure 31.N ₂ adsorption-desorption isotherm and (B) correlation coefficient curve in measurement of BET surface area of aged TP.....	98
Figure 32. Adsorption data and fitted isotherm models for copper with 25 mg aged TP. 99	
Figure 33. Adsorption data and fitted isotherm models for copper with 50 mg aged TP in 50 mL solution.	100
Figure 34.(A-B) Adsorption data and fitted isotherm models for copper with 100 mg untreated TP in 50 mL solution.	101
Figure 35(A-B) Adsorption data and fitted isotherm models for copper with 200 mg untreated TP in 50 mL solution.	102
Figure 36. (A-B) Adsorption data and fitted isotherm models for copper with 200 mg aged TP in 50 mL solution.....	103
Figure 37. Adsorption data and fitted isotherm models for lead with	104
Figure 38. Adsorption data and fitted isotherm models for lead with 50 mg untreated TP in 50 mL solution.	105
Figure 39.(A-B) Adsorption data and fitted isotherm models for lead with 25 mg untreated TP in 50 mL solution.	106
Figure 40. (A-B) Adsorption data and fitted isotherm models for lead with 50 mg aged TP in 50 mL solution.	107
Figure 41. (A-B) Adsorption data and fitted isotherm models for lead with 25 mg aged TP in 50 mL solution.	108
Figure 42. Particle size distribution of the finer portion of the aged TP measured by an optical microscope.	109

Chapter 1: Project Overview

Tire particles (TP) generated from synthetic rubber tires are classified into tire wear particles (TWP), recycled tire crumb (RTC), and tire repair-polished debris (TRD) (Luo et al., 2021). TWP are produced during friction between tires and road surface. RTC are used in artificial turfs, & playgrounds and TRD are produced during tire repair in auto shops (Luo et al., 2021). TWP emission is higher than the other two types of TP. TWP is divided into a) finer airborne and b) coarser non-airborne emissions. Airborne emissions are intensively studied compared to non-airborne emissions (Amato et al., 2014) (Grigoratos & Martini, 2015) (Thorpe & Harrison, 2008) (Wagner et al., 2018). This study was focused on non-airborne TWP.

According to the International Organization for Standardization (ISO), TP are not plastic since the rubber has reversible elastic deformation (*Plastics — Vocabulary*, 2013). However, Verschoor (2015) suggested that microplastics cover all synthetic macromolecular substances, which includes TP. When TP are considered microplastics, they amount to 70% of the microplastics in the environment (Lassen et al., 2012) (Fan et al., 2021) (Leads & Weinstein, 2019). They are the second largest source of microplastics in the ocean (Boucher & Friot, 2017). Since TP are not degradable, they can accumulate in the environment. The worldwide TP production in 2019 was estimated at 2.89×10^6 tons (Luo et al., 2021). Previous studies have revealed that tire materials leach zinc (Rhodes et al., 2012) (Degaffe & Turner, 2011) and toxic polycyclic aromatic hydrocarbons (PAHs) (Wachtendorf et al., 2017) to the environment. Tires have a weighted average zinc content of 1-2% (Rhodes et al., 2012). Tires are reported to

contain PAH content (Sadiktsis et al., 2012). Hence, the pollutants originate from tires. They can also cause toxic fumes through combustion containing hydrocarbon oil, carbon and sulfur (Ali et al., 2021). As a result, the disposal of TP is a great concern.

TP have complex composition. Their composition, size, functional groups, and surface roughness change as they age in the environment. TP are composed of styrene-butadiene rubber copolymer (SBR) or a mixture of rubber and SBR (Hüffer et al., 2019) (Lin & Teng, 2002). Generally, the rubber of tires consists of 60-65% SBR and natural rubber, 29-31% carbon black, 2-3% zinc oxide, and 1-2% sulfur (Lin & Teng, 2002). The behavior of TP changes with the process of generation and aging in the environment. As a result, the fate, transport, and behavior of TP in the environment are not well understood.

TP and heavy metals are two classes of contaminants. The interaction between them is not well understood. Several heavy metals (iron, zinc, copper, manganese, etc.) are essential to humans and plants at low concentrations. They are toxic when they exceed a specific allowable concentration. Other heavy metals (arsenic, cadmium, lead, thallium, mercury, etc.) are toxic at any concentration. Some heavy metals can also bioaccumulate. Ineffective industrial and domestic wastewater treatment leads to heavy metal contamination of rivers and oceans. Lead and copper were chosen as representative heavy metals in this study. Lead is found in the earth's crust. It is present in various products like paint, ceramics, plumbing materials, batteries, cosmetics, etc. Lead exposure at high levels can harm the kidneys and the brain, in addition to causing anemia and weakness. (Tong, 2000). Copper is a native metal since it is found in its pure,

metallic state in nature. It is widely used for wiring, plumbing, and making machine parts. Exposure to copper may cause harm to the liver, brain, and other organs (Gaetke, 2003).

Previous studies have reported that waste tire-derived activated carbon can be used in the removal of heavy metals (Al-Asheh & Banat, 2000) (Mousavi et al., 2010) (López et al., 2013) (Gupta et al., 2014) (Makrigianni et al., 2015). Very few studies have investigated the adsorption of heavy metals on TP (Fan et al., 2021) (Sivaraman et al., 2022). The focus of existing investigations of chemical sorption to tire materials have been in the area of water/wastewater treatment, where the main objective was to evaluate the performance of tire materials versus commercial sorbents to assess the effectiveness of removing contaminants from aqueous solutions. However, these studies limited the range of sorbates to relatively high concentrations and a narrow range of sorbent sizes. These limitations inhibited the comprehensive understanding of the environmental risk assessment of TP, especially for the adsorption-desorption process. It has been suggested that microplastics are vectors for heavy metals and organic contaminants (G. Liu et al., 2021) (Godoy et al., 2019) (Mosca Angelucci & Tomei, 2022). Vector means strong adsorbents of contaminants which can significantly change the bioavailability and toxicity of the contaminants. Like microplastics, the TP may have the potential to be vectors for heavy metals. An environmental risk assessment would be necessary if TP were vectors for heavy metals.

1.1 Objectives

This study aimed to investigate the adsorption of heavy metals on TP. A wide size range of TP and low concentration of heavy metal were used to understand the adsorption behavior in this study. The objectives of this study were 1) analyze adsorption data of lead and copper on TP (with or without aging) using adsorption models (Langmuir and Freundlich); 2) investigate competitive adsorption of lead and copper on aged TP; 3) evaluate the pH effect on the adsorption of heavy metal on aged TP; 4) investigate possible adsorption mechanisms involved in heavy metal adsorption on TP. The novelty of this study was 1) assessment of the potential of TP as vectors for heavy metals; 2) investigation of pH effect on adsorption of heavy metals on TP; 3) insight into possible mechanisms involved in the adsorption process. Figure 1 shows the summary of the research objectives and approach. TP were generated from the tire scraps from recycled tire and used in this study.

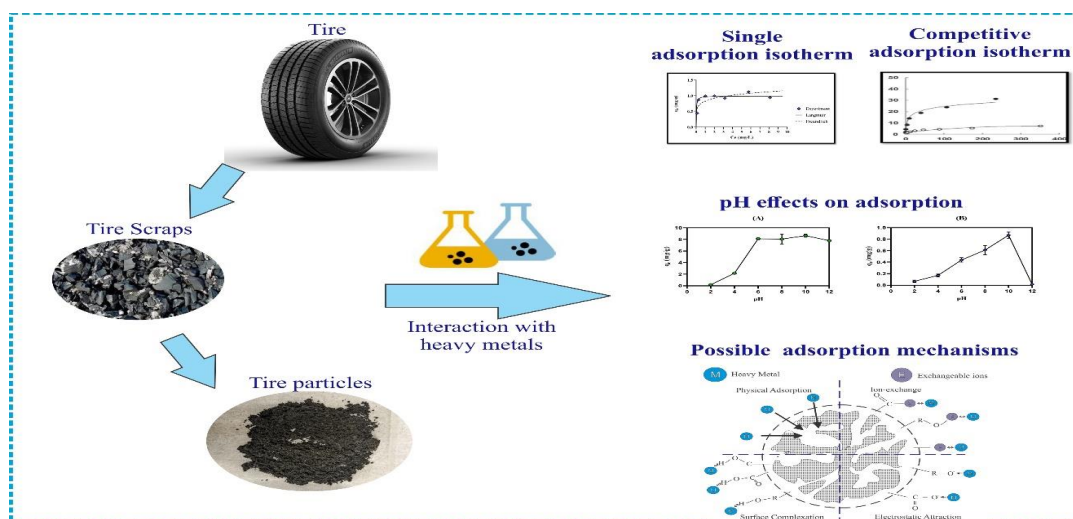


Figure 1. Summary of research objectives and approach.

Chapter 2: Literature Review

2.1 Generation of TP

The amount of TP generation depends on tire consumption, road conditions, climate, tire properties, etc. (Luo et al., 2021) (Baensch-Baltruschat et al., 2020). TWP are generated by mechanical abrasion during contact between tires and the road surface. During the friction, the non-exhaust particulate matter creates the airborne TWP. In addition to fine airborne emission, coarser non-airborne particles are generated due to heat and abrasive force. 90-99.9% of the TWP emissions are non-airborne (Panko et al., 2013). Figure 2 shows that the global TWP generation over the years steadily increased, and in 2019, it was estimated as 2.89×10^6 tons (Luo et al., 2021). The global average per capita TWP generation was estimated at 0.81 kg/year (Kole et al., 2017). The increasing trend of TWP generation indicates that they will be a significant problem in the future.

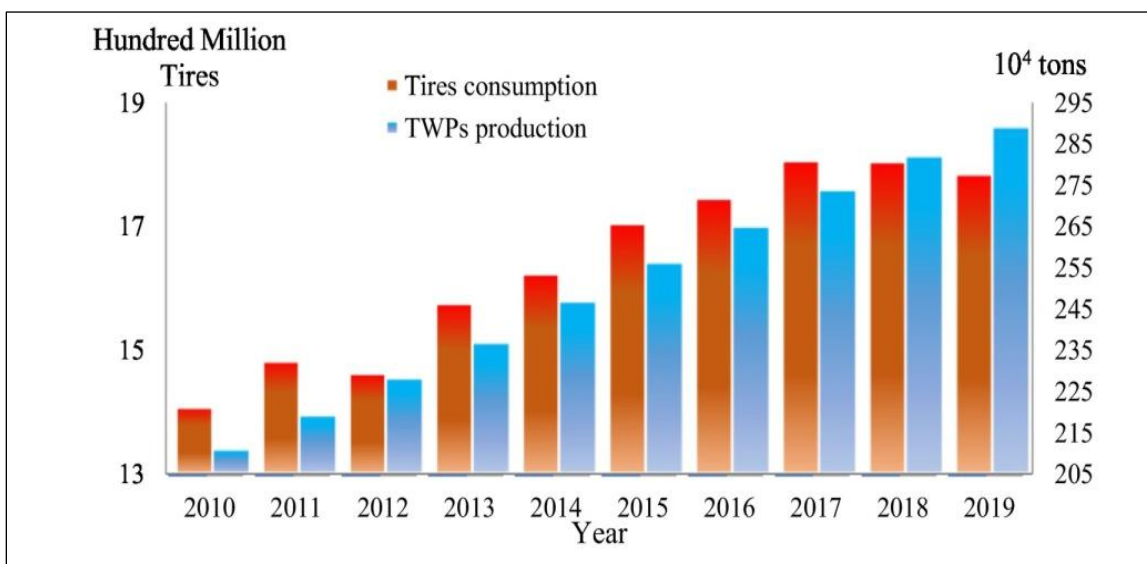


Figure 2. The global TWP generation steadily increased over the years

(reproduced from Luo et al., 2021).

To date, the TP used in studies to represent TWP are generated from a) cryo-milling of the tire, b) road simulators, or c) environmental samples. The TP generated from the three processes differ in physical and chemical properties. Collecting TWP from the environment is difficult, and the sampling process may change the properties. The challenge of using TWP from road simulators is the high technical requirement. Comparatively, the generation of cryo-milled TWP is easier, and the properties of the particles are uniform. In this study, cryo-milled TWP were used. The downside of using cryo-milled TP is that they are not heteroaggregates like environmental TWP.

2.2 Properties of TP

A few studies reported comparisons among different TP (European Commission. Joint Research Centre. Institute for Energy and Transport., 2014) (Kim & Lee, 2018) (Kreider et al., 2010) (Lee et al., 2013) (Klößner, Seiwert, Weyrauch, et al., 2021) (Wagner et al., 2022). Table 1 shows the difference in physical and chemical properties in three differently generated TP. The density of TWP from road simulators and TWP from the environment (1.3–1.9 g/cm³) were higher than the cryo-milled TP (1.2 g/cm³). TWP can form heteroaggregates combined with dust and minerals derived from road surface. (Baensch-Baltruschat et al., 2020) (Kreider et al., 2010)(Sommer et al., 2018). The increase in density is attributed to the presence of dust and minerals in the TWP from road simulators and the environment (Kreider et al., 2010).

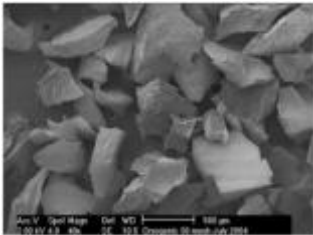
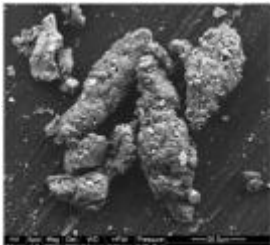
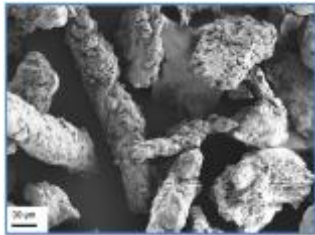
	Cryo-milled TP	TWP from road simulators	TWP from environmental
Shape			
	Reprinted from (Pehlken & Elhachmi Essadiqi, 2005)	Reprinted from (Kreider et al., 2010)	Reprinted from (Klöckner, Seiwert, Weyrauch, et al., 2021)
Size range	Micrometer	Nano- to micrometer	Nano- to micrometer
Density range	1.2 g/cm ³	1.7–1.9 g/cm ³	1.3–1.9 g/cm ³
Shape	Irregular (no elongated)	Elongated (a few irregular)	Elongated (a few irregular)
Composition	Consist of nothing bur rubber. •Composition depends on aging.	•Consist of both rubber and dust	•Consist of rubber, mineral particles, and dust. •Composition changes with different types of aging.

Table 1. Comparison among the size, shape, and density of differently generated TP

(reproduced from Wagner et al., 2022)

2.2.1 Chemical Composition

Tire rubber is mainly a mixture of synthetic polymer SBR and natural rubber (Hüffer et al., 2019) (Lin & Teng, 2002). The other ingredients include polybutadiene, chloroprene-isoprene, polysulfide, carbon black, and silica (Guzmán et al., 2013). Different additives are also used to enhance performance. The additive includes mineral oils, different organic compounds, zinc oxide, sulfur, selenium, etc. (González et al., 2012). Figure 3 (A-B) shows the basic structure and percentage of different materials of tire. The properties of TWP are different based on the process of generation. TP are reported to leach Zn (Rhodes et al., 2012) (Degaffe & Turner, 2011) and PAHs (Wachtendorf et al., 2017) to the environment. Tires have a weighted average zinc content of 1-2% (Rhodes et al., 2012). Tires are reported as a potential source of carcinogenic dibenzopyrenes (PAH) to the environment (Sadiktsis et al., 2012). Some studies analyzed tire treads and found the presence of hundreds of compounds, and most of the compounds were unknown. The unknown compounds were suggested to be formed during the usage/production process and thought to be transformation products (Halle et al., 2021) (Klößner, Seiwert, Wagner, et al., 2021) (Müller et al., 2022). TWP from the environment form heteroaggregates combining with dust and mineral particles from road surfaces (Baensch-Baltruschat et al., 2020) (Kreider et al., 2010)(Sommer et al., 2018).

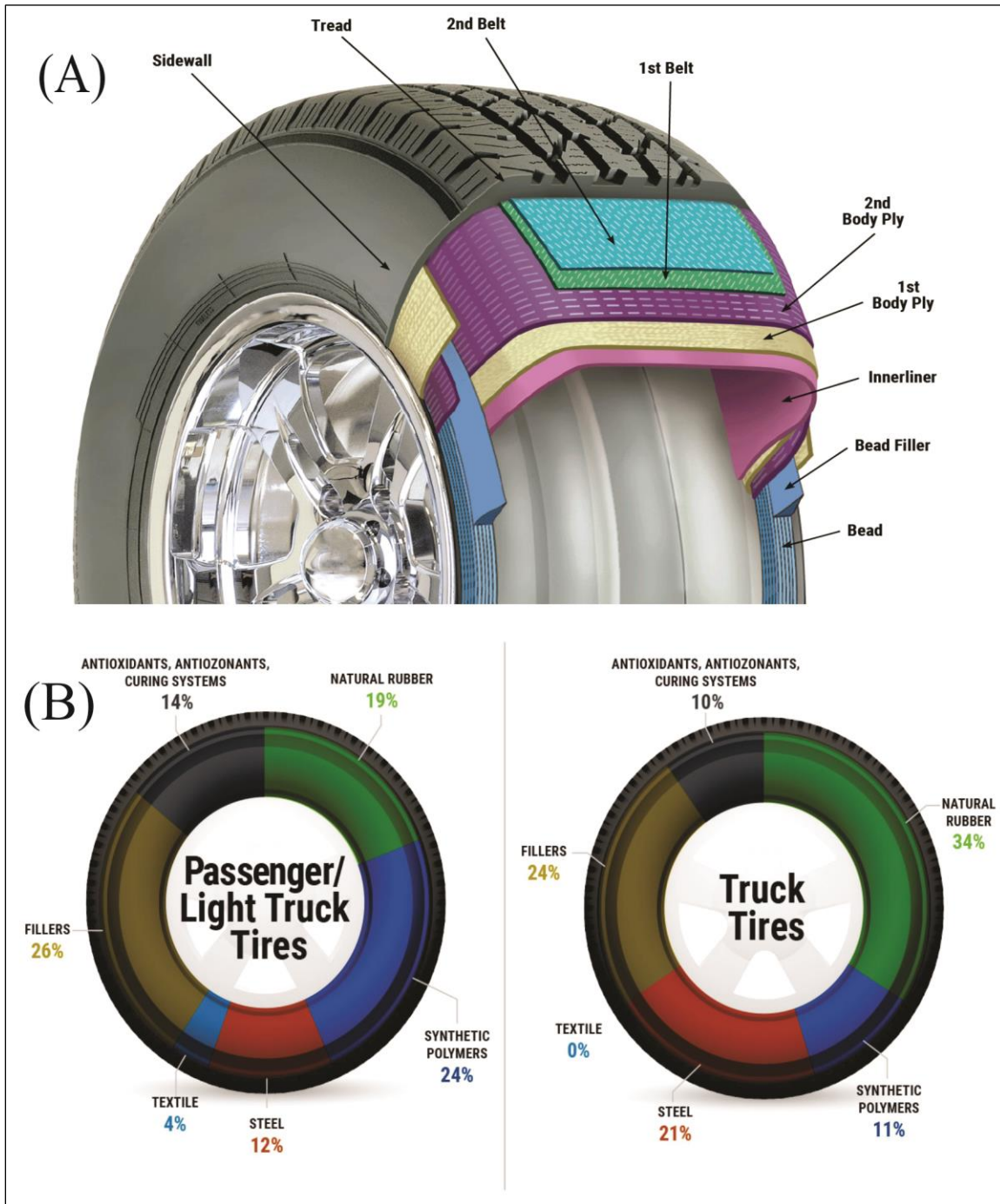


Figure 3. A) Basic sections of a tire. B) Percentage of different components of tires (reproduced from *What's In a Tire* | U.S. Tire Manufacturers Association, n.d.)

2.2.2 Size Distribution

The size of microplastics is regarded as 5mm to 1 μ m (Hüffer et al., 2017). The size reported for TP ranged from a few nanometers to 265 μ m (Kreider et al., 2010) (Valente & Sibai, 2019) (Wagner et al., 2018) (Luo et al., 2021). The TWP generated from different process vary in size. The size of the TWP generated from a road simulator was reported to be 0.5 μ m to 220 μ m with a maximum amount in the 70-80 μ m range (Kreider et al.,2010). The size distribution of TWP from the on-road driving test was reported in the range of 50 nm-20 μ m (Kwak et al., 2013).

2.2.3 Surface Properties

Scanning electron microscope (SEM) imaging was used to evaluate the surface morphology of the TP. The cryo-milled TP were irregular in shape without any elongated particles (Pehlken & Elhachmi Essadiqi, 2005). On the contrary, the TWP from the road simulators and the environment were elongated, and some of the particles were irregular (Kreider et al., 2010) (Klößner, Seiwert, Weyrauch, et al., 2021). SEM was also used in this study to investigate the morphology of the TP.

Fourier Transform Infrared Spectroscopy (FT-IR) is a useful technique to analyze the surface functional groups on TP. Sivaraman et al. (2022) reported the presence of -C=O (carboxyl), -C_nH_{2n+1} (alkyl), -NH₂, and -OH (hydroxyl) groups on the TP surface. FT-IR was used to analyze the TP used in this study.

2.3 Comparison of TP with Microplastics in Adsorption of Heavy Metals

Microplastics are attributed as vectors for organic contaminants (Velzeboer et al., 2014) and heavy metals (Brennecke et al., 2016). Vector refers to strong adsorbents which can significantly alter the bioavailability and toxicity of the contaminants. As a result, microplastics can be harmful to both aquatic organisms and human health (Vethaak & Leslie, 2016). Research is needed to investigate if TP may play similar roles. Some argue that microplastics are not a vector since they are outcompeted as sorbents by particulate matter, which are in far greater quantity (Koelmans et al., 2016). Microplastics show better adsorption capacity than particulate matter in nature (Koelmans et al., 2016).

In examining the vector effect of microplastics for heavy metals, isotherm experiments were conducted, and partitioning data were fit into adsorption models. Table 2 reports a few Langmuir and Freundlich model parameters for lead and copper adsorption on a few common microplastics. In comparison to the adsorption capacity of microplastics for heavy metals, the adsorption capacity of TWP was higher (Fan et al., 2021) (Sivaraman et al., 2022). In this study, Langmuir and Freundlich model parameters were calculated and compared with those of microplastics to examine the potential of TP as vectors of heavy metals. Previous studies used a narrow range of TWP sizes and high heavy metal concentrations. In the adsorption experiments in this study, the heavy metal concentration used were 1,2,3,4,5,8 and 10 mg/L. The concentration is much higher than the concentration in the environment. Using high concentrations of heavy metals is common for adsorption experiments (Fan et al., 2021) (Sivaraman et al., 2022) (Park et al., 2016) as the detection of lower concentrations is difficult. 48h was chosen as the

Heavy metal	Adsorbent	Langmuir			Freundlich			Reference
		Q_m (mg/g)	b_a (L/mg)	R^2	K_f $\frac{\text{mg/g}}{(\text{mg/L})^{1/n}}$	$1/n$	R^2	
Pb	Polystyrene (PS)	0.160	1.81	0.977	0.109	1.718	0.993	(Mao et al., 2020)
	PS (UV 3 months)	0.202	2.56	0.989	0.154	1.912	0.995	
Cu	PS	0.210	0.502	0.982	0.070	1.342	0.991	(Mao et al., 2020)
	PS (UV 3 months)	0.173	1.34	0.979	0.101	1.704	0.995	
Cu	Polyethylene terephthalate (PET) (Aged UV)	0.357	0.176	0.86	1.650	0.538	0.78	(Wang et al., 2020)
Pb	PS	2.94	1.07	0.999	1.33	0.255	0.945	(Godoy et al., 2019)
	polyethylene (PE)	2.36	0.515	0.985	0.802	0.326	0.871	
	polypropylene (PP)	5.55	0.123	0.981	0.915	0.478	0.969	
Cu	PS	0.358	2.01	1.00	0.233	0.144	0.779	(Godoy et al., 2019)
	PE	0.259	1.39	0.999	0.165	0.145	0.638	
	PP	2.95	0.156	0.986	0.520	4.74	0.959	

Table 2. Langmuir and Freundlich parameters for lead and copper adsorption on microplastics.

equilibrium time in this study. 48h is known to ensure equilibrium for microplastics (Mao et al., 2020) (Godoy et al., 2019) (Fan et al., 2021). The interactions of microplastics with heavy metals and the mechanisms involved in the process have been extensively studied (Cao et al., 2021) (Ashton et al., 2010) (Holmes et al., 2012) (Turner & Holmes, 2015) (Tang et al., 2021). However, the mechanisms involved in the heavy metal adsorption on TP is not well investigated.

2.4 Heavy Metal Removal by Typical Adsorbents

Heavy metals can be removed by typical adsorbents (activated carbon, zeolite, silica gel etc.). Different modifications are often used to enhance the performance of the adsorbents. As a recycling measure for waste tires, tire-derived activated carbon has been used to remove heavy metals (Shahrokhi-Shahraki et al., 2021) (Al-Asheh & Banat, 2000) (Mousavi et al., 2010). Table 3 shows the Langmuir and the Freundlich model parameters for lead and copper removal by typical adsorbents and tire-derived activated carbon.

Adsorbent	Heavy metal	Langmuir			Freundlich			Reference
		Q _m (mg/g)	b _a (L/mg)	R ²	K _f $\frac{\text{mg/g}}{(\text{mg/L})^{1/n}}$	1/n	R ²	
Activated Carbon (AC)	Pb	21.88	3.51	0.997	11.49	0.409	0.858	(Goel et al., 2005)
	Pb	42.50	0.008	0.971	3.87	0.31	0.977	(Shahrokhi-Shahraki et al., 2021)
	Cu	15	0.003	0.971	2.31	0.21	0.987	(Shahrokhi-Shahraki et al., 2021)
Tire-derived AC	Pb	322.50	0.015	0.978	78.50	0.19	0.748	(Shahrokhi-Shahraki et al., 2021)
	Cu	185.20	0.005	0.975	20.20	0.27	0.906	(Al-Asheh & Banat, 2000)
	Cu (303K)	20.31	0.039	0.978	0.931	0.788	0.993	(Mousavi et al., 2010)
Silica gel/chitosan composite	Pb (303K)	416.67	0.0043	0.992	42.072	0.306	0.999	(Rajiv Gandhi & Meenakshi, 2012)
	Cu (303K)	2000	0.003	0.991	22.12	0.067	0.999	(Zou et al., 2006)
MnO ₂ coated Zeolite	Pb (303K)	60.08	0.066	0.998	52.84	0.196	0.912	(Zou et al., 2006)
	Cu (303K)	8.127	0.212	0.988	10.46	0.244	0.940	

Table 3. Langmuir and Freundlich model parameters for lead and copper adsorption on commercial adsorbents and tire-derived activated carbon.

2.5 Competitive Adsorption

Competitive adsorption can show the selectivity sequence of heavy metals for an adsorbent. For tire-derived activated carbon, the reported selectivity sequence was $Pb > Cu > Zn$ (Shahrokhi-Shahraki et al., 2021). The selectivity sequence of heavy metals is case-specific (Park et al., 2016) (Schwertmann et al., 1989). In this study, the preference for adsorption on TP between lead and copper was investigated

The adsorption capacity of adsorbents is affected by the presence of other metals. Tire-derived activated carbon showed a reduction in capacity due to the presence of other heavy metals compared to the capacity in the single metal system (Shahrokhi-Shahraki et al., 2021). In this study, the effect on the adsorption capacity of TP due to competitive adsorption was investigated.

2.6 Aging of TP

Aging can change the behavior of TP through different processes. The aging can change the size, shape, surface roughness, and functional groups of TWP depending on the aging process. The main aging processes for TP are oxidation, shear stress, leaching, and microbial degradation (Wagner et al., 2022). Photooxidation may change the composition and surface properties (functional groups) of TP (Kolomijeca et al., 2020) (Unice et al., 2015). Shear stress influences particle size by breaking up particles or aggregating particles. Microbial degradation may increase hydrophilicity and surface roughness (Aboelkheir et al., 2019). Mineralization of rubber may also be possible through biodegradation (Cadle & Williams, 1980). Leaching of contaminants from TP to the environment is also reported (Rhodes et al., 2012) (Degaffe & Turner, 2011)

(Wachtendorf et al., 2017). Aging can change the adsorption of heavy metals on TP. Fan et al. (2021) reported UV aging increased surface area and changed surface functional groups of TWP, which resulted in higher adsorption of heavy metals.

Oxidation by nitric acid is known to change the physical and structural properties of plastic-derived materials (Rosca et al., 2005) (Cho et al., 2008). To mimic the oxidation process in the environment, the untreated TP were aged with 30% nitric acid in this study.

2.7 Fate and Transport of Heavy Metals Affected by Adsorption on TP

The waste tire-derived activated carbon effectively removed organic pollutants (Makrigianni et al., 2015) (Gupta et al., 2014), dye (Makrigianni et al., 2015) (López et al., 2013), and heavy metals (Karmacharya et al., 2016) (Al-Asheh & Banat, 2000) (Mousavi et al., 2010). TP were also used for the removal of heavy metals (Fan et al., 2021) (Sivaraman et al., 2022).

Heavy metals are less soluble in water and tend to adsorb onto particulate matter or bind to organic compounds. Under normal circumstances, elementary lead and copper do not dissolve in water. Water soluble compounds lead nitrate (solubility: 50 g in 100 mL cold water) and copper chloride (solubility: 75.7 g in 100 mL water at 25 °C) were used in this study. The fate and transport of heavy metals can be affected by the presence of strong adsorbents. Heavy metals are thought to be virtually immobile in the subsurface/surface water, if they quickly bind to immobile aquifer media (McCarthy & Zachara, 1989). However, colloids in the solid phase may be mobile, which could sorb heavy metals and stabilize them in the mobile phase (McCarthy & Zachara, 1989). The

amount of contaminants that the subsurface/surface flow can carry can increase due to the colloids. Colloidal transport can be a dominant mechanism for heavy metals as a result. Stable suspended colloidal material is necessary to facilitate contaminant transport over a long distance (McCarthy & Zachara, 1989). Colloids that are stable are not susceptible to aggregation. Colloid stability is influenced by factors like density, size, surface chemistry, water chemistry, etc (McCarthy & Zachara, 1989). TP are a new source of mobile organic colloids which can facilitate heavy metal transport. It is unclear if TP can create stable colloids for contaminant transfer.

Like microplastics, TP may accumulate a variety of heavy metals and may release the adsorbed heavy metals from the surface of TP. The adsorption-desorption process can alter the concentration of heavy metals in the environment. There can be a significant change in the concentration of heavy metals in sediment/organisms due to the presence of TP in them. The adsorption of heavy metals on TP may modify the toxicity. Heavy metals are toxic when they exceed a specific concentration. Heavy metals can be harmful to wildlife and human due to adsorption on TP and exceeding the specific concentration (Pachana et al., 2010). The toxicity may increase due to the presence of two co-existing contaminants. Other contaminants had exhibited similar behavior (Abdolahpur Monikh et al., 2020). An updated risk assessment may be required for the heavy metal adsorption on TP. Adsorption on TP can increase the mobility of adsorbed heavy metals. The adsorbed heavy metals can migrate and accumulate in the soil. The accumulated metals may get into the food chain which may have significant effect on wildlife and humans.

2.8 Mechanisms in Heavy Metal Adsorption on TP

TP are composite sorbents containing a small percentage of carbon black compared to the rubber matrix. Sorption to tire crumb for organic compounds is interpreted as a combination of adsorption and absorption.

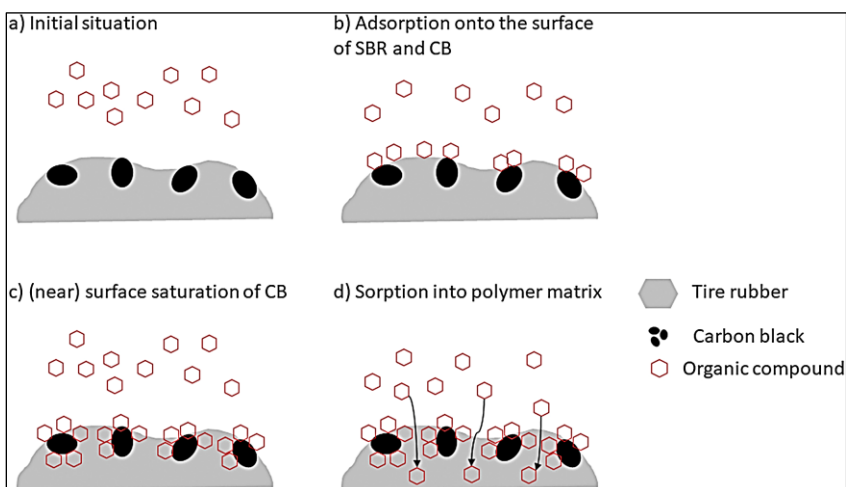


Figure 4. Sorption mechanism of organic compounds on tire crumb rubber (reproduced from Hüffer et al., 2019).

The sorption of organic compounds to carbon black was attributed to adsorption, and for the rubber matrix it was absorption (Alamo-Nole et al., 2012) (Figure 4). It is unclear if heavy metals are absorbed in the TP. More studies are required to elucidate the mechanisms. Adsorption is regarded as the main mechanism for heavy metal sorption on TP. For conventional adsorbents, four mechanisms are considered to be involved during heavy metal interaction with them. The mechanisms are 1) physical interaction, 2) ion exchange, 3) electrostatic interaction, and 4) interaction through surface complexation (Figure 5).

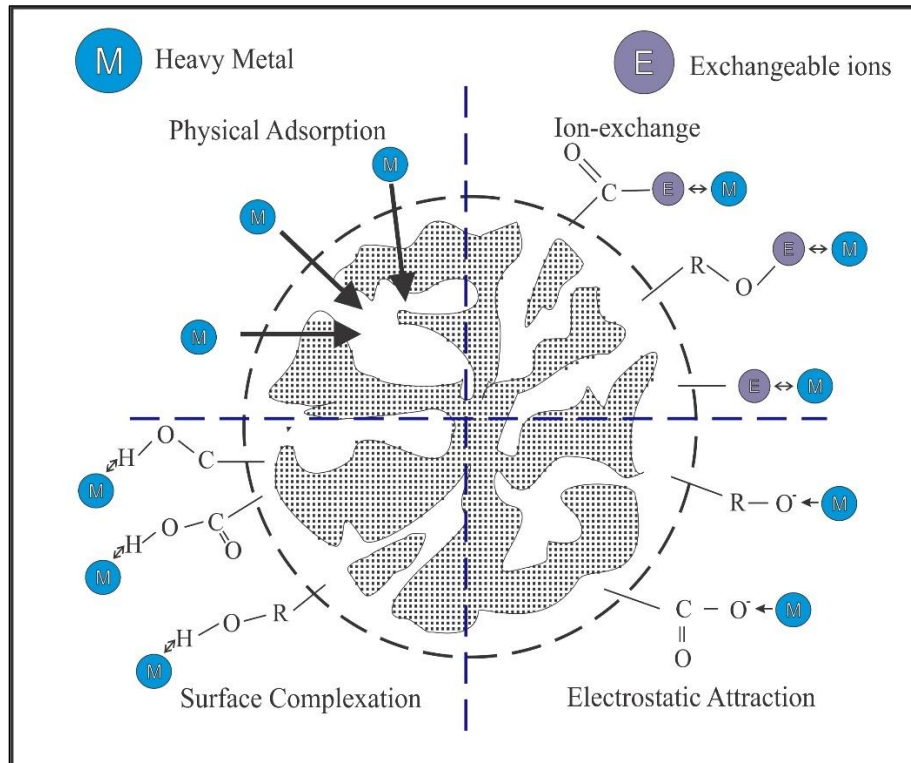


Figure 5. The possible mechanisms involved in heavy metal adsorption on typical adsorbents.

For adsorption of heavy metals on microplastics, these 4 mechanisms and co-precipitation are considered (S. Liu et al., 2022). The physical adsorption increases as surface area of adsorbents increase. The relationship between surface area of the adsorbents and other mechanisms (ion exchange, electrostatic attraction, surface complexation) is unclear. More studies are needed to investigate the relationship. For microplastics and tire-derived activated carbon, electrostatic interaction and surface complexation were the major mechanisms involved in heavy metal adsorption (Shahrokhi-Shahraki et al., 2021) (Cao et al., 2021). However, it is unclear if the

interaction between heavy metals and TP follows the same mechanisms. However, the mechanisms involved in the heavy metal adsorption on TP is not well investigated.

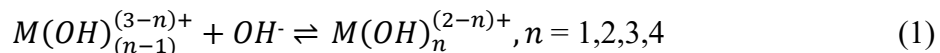
2.9 Influence of Environmental Factors

Environmental factors like pH, ionic strength, presence of organic matter, and presence of other contaminants can influence heavy metal adsorption on TP. pH is one of the most important environmental factors influencing heavy metal adsorption. pH can change the surface charge of TP. Metal species in water also change with pH. pH may influence ion exchange, electrostatic interaction, and surface complexation mechanisms in heavy metal adsorption on TP.

2.9.1 Effect of pH on Heavy Metal Adsorption on TP

Previous studies have investigated the pH effect on heavy metal adsorption with microplastics (Fu et al., 2021), tire-derived activated carbon (Karmacharya et al., 2016), and different adsorbents (Abollino et al., 2003) (Chen et al., 1997). However, the effect of pH variation on the adsorption of heavy metals on TP was not reported.

Divalent metal ions, like copper and lead, go through hydrolysis processes in the aqueous solution that can be represented as

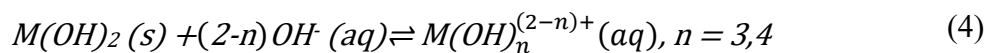
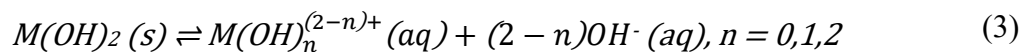


A series of equilibrium expressions of the following form describe the distribution of the various hydroxy species at pH levels where metal hydroxide does not precipitate.

$$K_n = \frac{[M(OH)_n^{(2-n)+}]}{[M(OH)_{(n-1)}^{(3-n)+}] \cdot [OH^-]} \quad (2)$$

Where K_n = stepwise equilibrium constant

Each soluble hydroxy species' concentration is controlled by its solubility product when solid metal hydroxide is present. The following equilibria are valid, assuming that $M(OH)_2$ is the only solid that has formed.



Equations of the following form are used to determine the concentrations of soluble species.

$$K_{sn} = [M(OH)_n^{(2-n)+}] \cdot [OH^-]^{(2-n)} \quad (5)$$

Table 4 shows the stability equilibrium constants for Cu (II) and Pb (II) at 25°C. A higher stability equilibrium constant means that the ion is more stable and easily formed.

Cation	Stability constant	At temperature 25°C
Cu (II)	K ₁	6.8
	K ₂	6.9
	K ₃	1.3
	K ₄	1.0
	K _{s1}	-12.2
	K _{s2}	-5.3
	K _{s3}	-4.0
	K _{s4}	-3.0
	K _{sp}	-19.0
	Pb (II)	K ₁
K ₂		6.3
K ₃		2.8
K ₄		0.9
K _{s1}		-10.7
K _{s2}		-4.4
K _{s3}		-1.6
K _{s4}		-0.7
K _{sp}		-17.0

Table 4. Stability constants (logarithms to base 10) for copper (II) and lead (II) at 25°C

(reproduced from Rodda et al., 1993).

The nature of the metal species in water depends on pH. Figure 6 shows the presence of different species of lead and copper as a function of pH. The surface charge of the adsorbent also changes with pH. The adsorbent is positively charged below the

point of zero charge (pHpzc) and negatively charged above pHpzc. For electrostatic interaction, both the surface charge of the adsorbent and the charge of the metal species in the water sample are important factors. Figure 6 (A) shows that at $\text{pH} \leq 7.5$, the major fraction is Pb^{2+} . At $7.5 \leq \text{pH} \leq 9.5$, $\text{Pb}(\text{OH})^+$ species dominates. At $9.5 \leq \text{pH} < 11.2$, the predominant lead species is $\text{Pb}(\text{OH})_2(\text{aq})$. At $\text{pH} \geq 11.2$, $\text{Pb}(\text{OH})_3^-$ dominates.

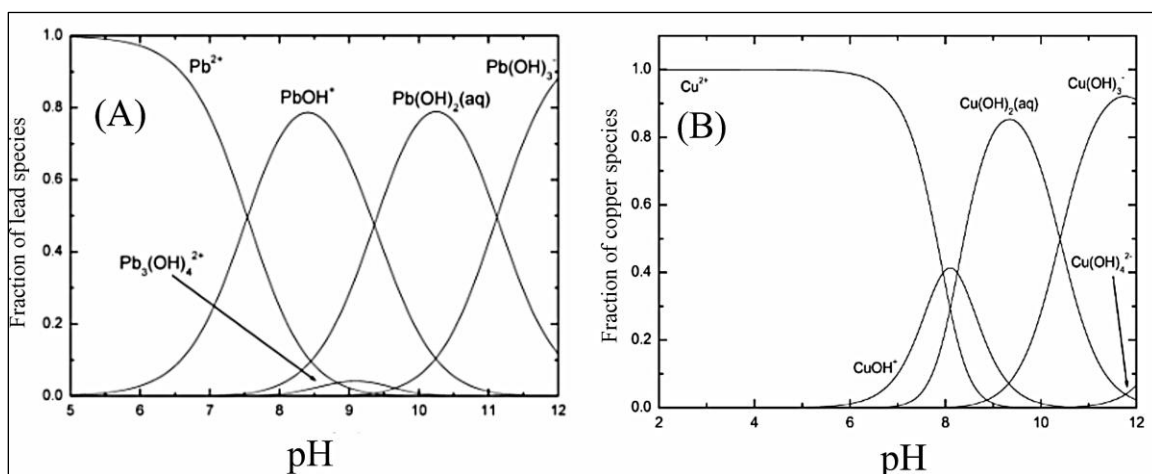


Figure 6. (A) Lead (reproduced from Powell et al., 2009) and (B) copper (reproduced from Powell et al., 2007) species in aqueous solution as a function of pH.

Figure 6 (B) shows that at $\text{pH} \leq 7.8$, the dominant copper species is Cu^{2+} . At $8.2 < \text{pH} < 10.2$, the major species is $\text{Cu}(\text{OH})_2(\text{aq})$. When $\text{pH} > 10.2$, $\text{Cu}(\text{OH})_3^-$ dominates. Apart from metal hydroxides, bicarbonates, Cl^- , SO_4^{2-} , and complexes of metals/natural organics are present in natural water. The interactions of these species were beyond the scope of the current project. More studies are needed to investigate the effect of

interactions of common complexes and ions present in natural water with adsorption of heavy metals on TP.

Chapter 3: Methodology

3.1 TP Preparation

TP used in this study were made from tire scraps from a playground. The playground was located at New Albany Links, New Albany, Ohio. The tire scraps were used in the surfacing of the playground. Approximately 1 kg of tire scraps was collected. The tire scraps were cleaned with deionized water (DI) to remove any dirt from the surface of the scraps and cut with scissors into small pieces (~10mm). The small pieces were cryo-milled by a mill machine (RETSCH ZM 200 Ultra Centrifugal Mill). The mill machine was located at Stocker 007, Ohio University. Liquid nitrogen is commonly used as a refrigerant in most size reduction procedures (Liang & Hao, 2000). The liquid nitrogen was collected in a specialized vacuum flask from the Life Sciences building at Ohio University. The specialized vacuum flask was borrowed from the electrical engineering department at Ohio University. The mill machine used rotors to grind the tire pieces, and much heat was produced in the process. With trial and error, the settings for the mill machine were chosen. The mill machine was operated at 6000 rpm for 10-15 seconds for grinding each batch of tire pieces. Increasing the rotor speed or time resulted in the melting of the TP. The tire pieces were soaked in liquid nitrogen, and around 15 mg of tire pieces were fed into the rotor using a spoon in each batch. The tire pieces were ground into TP under a cryogenic state. The TP generated were named untreated TP. Figure 7 shows different equipment used in the preparation of TP.

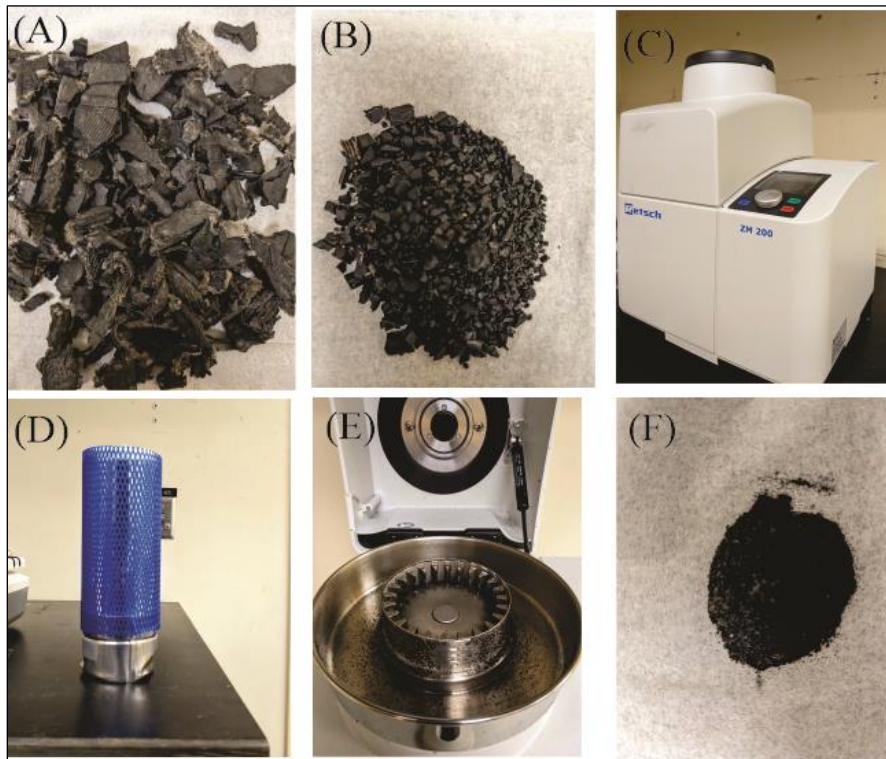


Figure 7. (A) Tire scraps collected from the playground. (B) Small pieces of tire scraps (~10mm). (C) Mill machine (RETSCH ZM 200 Ultra Centrifugal Mill) used to make TP. (D) Liquid nitrogen used in milling. (E) TP generated in the mill machine. (F) Aged TP.

3.2 Preparation of Aged TP

TP age through oxidation, shear stress, leaching, and microbial degradation in the environment (Wagner et al., 2022). Typically, aging or weathering processes in the natural environment are technically considered oxidation processes which, in general, result in physical and chemical changes in the particles. Real-time investigation of the weathering effects on these changes is expensive and time-consuming. Thus, it has been a common practice in the literature to utilize oxidants or acids as an alternative to mimic

the effects of the natural aging process. Oxidation by nitric acid is known to change the physical and structural properties of plastic-derived materials (Rosca et al., 2005) (Cho et al., 2008). To mimic the oxidation process in the environment, the untreated TP were soaked in 30% nitric acid for 24h. Then the particles were cleaned with DI water several times and vacuum filtered. Next, the particles were dried in an oven at 100° C for 24 h. The TP particles obtained from the process were named aged TP and stored in an airtight beaker.

3.3 Batch Adsorption Tests

One of the most typical tests used to evaluate adsorption equilibrium from solutions is a batch adsorption experiment. The experiment is repeated while changing the amount of solid, the initial concentration of the solution, or both in order to establish an adsorption isotherm. The variation in the amount of adsorbate that the adsorbent adsorbs with temperature and constant pressure is expressed by the curve known as the adsorption isotherm. The affinity of an adsorbate for an adsorbent is computed using isotherms. In this study, sorption data of heavy metals on TP were analyzed using Langmuir and Freundlich models. When estimating model parameters, nonlinear regression is more precise than linear (Chen et al., 2022). Non-linear regression was used in this study. The Langmuir and Freundlich isotherm equations are as follows:

$$\text{Langmuir: } q_e = \frac{Q_M b_a C_e}{1 + b_a C_e}$$

Where C_e = equilibrium concentration of adsorbate in solution, mg/L

q_e = equilibrium adsorbent-phase concentration of adsorbate, mg adsorbate/g adsorbent

b_a = Langmuir adsorption constant of adsorbate, L/mg

Q_M = maximum adsorbent-phase concentration of adsorbate when surface sites are saturated with adsorbate, mg adsorbate/g adsorbent.

$$\text{Freundlich: } q_e = K_f C_e^{1/n}$$

where K_f = Freundlich adsorption capacity parameter, (mg/g) (L/mg)^{1/n}

1/n = Freundlich adsorption intensity parameter, unitless

The equilibrium adsorbent-phase concentration of adsorbate (q_e) was calculated using the following formula:

$$q_e = \frac{(C_i - C_e)V}{m}$$

where, C_i = initial aqueous-phase concentration of adsorbate, mg/L

V = volume of aqueous phase added to the tube, L

m = mass of adsorbent, g

3.3.1 Single Batch Adsorption Tests

The representative heavy metals, lead, and copper solutions were prepared by dissolving $\text{Pb}(\text{NO}_3)_2$ and $\text{CuCl}_2 \cdot 2\text{H}_2\text{O}$ in DI water. Adsorption isotherm experiments were run with 50 mL heavy metal solutions in centrifuge tubes with concentrations of 1,2,3,4,5,8 and 10 mg/L. A single metal was evaluated during a single adsorption test. The pH of the heavy metal solution was 6.2. Through screening tests (Appendix B), the adsorbent dose for lead and copper was chosen to be 25 and 200 mg, respectively. Initially, in the screening tests, the adsorbent dose for copper was 25, 50, and 100 mg. It was difficult to get a robust curve keeping the initial copper concentration (1,2,3,4,5,8 and 10 mg/L) constant with adsorbent dose 25, 50, and 100 mg,-since there was a considerable difference among q_e values at different C_e . Non-linear regression was used

in this study. Regression models are sensitive to outliers. It was imperative to refrain from using the q_e values when they had a considerable difference among them. When the adsorbent dose was increased to 200 mg for copper, the difference among different q_e values decreased, resulting in a robust curve. For lead, 100, 50, and 25 mg adsorbent doses were tested, keeping lead concentration (1,2,3,4,5,8 and 10 mg/L) constant. 25 mg adsorbent produced satisfactory data for the regression model. 25 mg adsorbent dose was chosen for lead adsorption tests. Both untreated and aged TP were used in the single batch adsorption tests. Each test was conducted twice to check the reproducibility. Table 5 shows the adsorbent dose and heavy metal concentration used in single batch adsorption tests.

Heavy metal	Adsorbent	Adsorbent dose	Heavy metal concentrations	Volume of Heavy metal solution	No of replicates
Pb	Untreated TP	25 mg	1,2,3,4,5,8 and 10 mg/L	50 mL	2
	Aged TP				
Cu	Untreated TP	200 mg	1,2,3,4,5,8 and 10 mg/L	50 mL	2
	Aged TP				

Table 5. Adsorbent dose and heavy metal concentrations used in single batch adsorption tests.

Figure 8 shows different equipment used in the batch adsorption tests. The centrifuge tubes with heavy metal solution and TP were placed in an orbital shaker at 150 rpm for

48 h. After the elapsed time, the samples were centrifuged at 4000 rpm for 15 mins. The samples were filtered with a 0.45 μ m membrane filter.

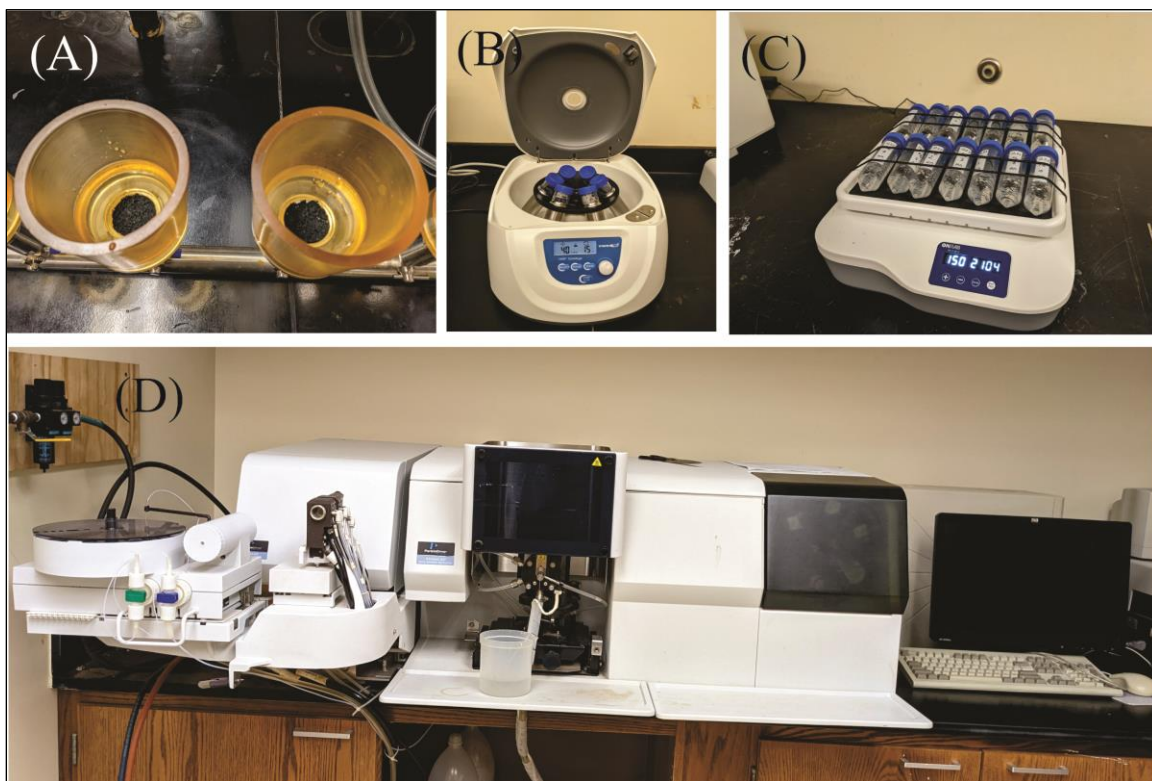


Figure 8. (A) Vacuum filtration of TP in the aging process. (B) Centrifuge used to separate TP and adsorbate. (C) Orbital shaker used to mix TP and adsorbate. (D) AAS machine used in measuring equilibrium aqueous phase concentration of adsorbate.

The metal concentration of the filtrates was measured with atomic absorption spectroscopy (AAS). The machine (PERKIN ELMER AANALYST 300) was located at Stocker 007 at Ohio University. For the measurement with the AAS machine, a calibration curve was generated. The standard concentrations used in the calibration

curve were 1,2,4,6,8 and 10 mg/L. The standards for the calibration were made from standard solutions for AAS. Each sample was analyzed three times in the AAS machine. All the chemicals used in this study were purchased from Fisher Scientific (US).

3.3.2 Competitive Adsorption Tests

For competitive adsorption, a dual-metal system with lead and copper was used. The lead and copper solutions were prepared by dissolving $\text{Pb}(\text{NO}_3)_2$ and $\text{CuCl}_2 \cdot 2\text{H}_2\text{O}$ in DI water. The aged TP were used in the competitive adsorption tests. The experiments were run with 50 mL heavy metal solution with concentrations of 1,2,3,4,5,8 and 10 mg/L. The pH of the heavy metal solution was 6.2. Table 6 shows the adsorbent dose and heavy metal concentration used in competitive batch adsorption tests.

Heavy Metals	Adsorbent	Adsorbent dose	Heavy metal concentrations	Volume of Heavy metal solution	No of replicates
Pb & Cu	Aged TP	25 mg	1,2,3,4,5,8 and 10 mg/L	50 mL	2
Pb & Cu	Aged TP	200 mg	1,2,3,4,5,8 and 10 mg/L	50 mL	2

Table 6. Adsorbent dose and heavy metal concentrations used in competitive batch adsorption tests.

Lead and copper concentrations in a sample were equal in competitive adsorption tests. The adsorbent dose was 25 and 200 mg for competitive isotherm for lead and copper,

respectively. In the mixed solution, lead adsorption was analyzed when the adsorbent dose was 25mg. When the adsorbent dose was 200 mg, copper adsorption was analyzed in the competitive adsorption test. This was done to contrast the single adsorption isotherm with the competitive batch isotherm. In the single adsorption tests, the adsorbent dose for lead and copper tests was 25 and 200 mg, respectively. That's why, in the mixed solution, lead was measured when the adsorbent dose was 25 mg, and copper was measured when the dose was 200 mg. Each test was conducted twice to check the reproducibility.

The centrifuge tubes with heavy metal solution and aged TP were placed in an orbital shaker at 150 rpm for 48 h. After the elapsed time, the samples were centrifuged at 4000 rpm for 15 mins. The samples were filtered with a 0.45 μ m membrane filter. The metal concentration of the filtrates was measured with atomic absorption spectrometry (AAS). For the measurement with the AAS machine (PERKIN ELMER AANALYST 300), a calibration curve was generated. The standard concentrations used in the calibration curve were 1,2,4,6,8 and 10 mg/L. The standards for the calibration were made from standard solutions for AAS. Each sample was analyzed three times in the AAS machine.

3.4 Characterization of TP

3.4.1 Scanning Electron Microscope (SEM) Imaging

SEM analysis was performed on untreated and aged TP to understand the morphology of the tire particles. The SEM analysis can also help investigate the effect of the aging process on the morphology of the TP. The untreated and aged TP were collected in sealed tubes and delivered to the Institute for Sustainable Energy and the

Environment at Ohio University. Dr. Damilola Daramola's lab conducted the SEM analysis. Each sample was around 10 mg. The samples were put in an aluminum stub using a sticky carbon tab. The sticky carbon tab kept the samples fixed to avoid any vibrations. The sample was put in a chamber, and the height of the sample was not more than 10mm. The accelerating voltage was set at 12kV. A conductive gold coating was used to improve the image quality. For the image, the focus was set at a magnification of 100 times on a sharp feature. Using Stigmators, the clear possible image was found with trial and error. When the clarity was satisfactory, images were taken.

At the time of publication, the SEM/EDS test results for untreated TP, aged TP, lead-adsorbed TP, and copper-adsorbed TP samples were incomplete. The SEM images for untreated and aged TP were generated, and they were reported in the result section. Energy-dispersive-X-ray spectroscopy (EDS) is conducted simultaneously with SEM analysis. EDS is used to find the chemical elemental composition of materials. Results from SEM/EDS can provide insight into how the morphology and chemical elemental composition changed before and after adsorption. The change can also be seen for before and after aging of the TP.

3.4.2 Brunauer-Emmet-Teller (BET) Surface Area

BET surface area was calculated for untreated and aged TP. 200 mg of untreated and 200 mg of aged TP were collected in sealed tubes and delivered to the Institute for Sustainable Energy and the Environment, Ohio University. The BET apparatus (Micromeritics ASAP 2020) was operated by Ahmad Abu Hajer (Ph.D. student from Dr. Jason Trembly's group). The samples were degassed for 5h at 200 °C under vacuum on

two separate occasions before measurement. Afterward, N₂ adsorption and desorption were conducted. The relative pressure (P/P_0) used in the test was 0.01 to 0.10. Using software from Micromeritics, the surface area was calculated.

Limitations. In BET measurement, the correlation coefficient for untreated and aged TP was 0.95777 and 0.9946, respectively. A correlation coefficient of 0.9999 is considered satisfactory for reliable BET measurement. During degassing for 5h at 200 °C under vacuum, oil content came out of the TP. Degassing the samples before BET measurement ensures the removal of moisture and other contaminants and accurate measurement of the surface area. The oil content may have been an additive during the tire manufacturing process. Oil content on the TP can interfere with the BET measurement. The samples were degassed for another 5h at 200 °C under vacuum to ensure no more oil coming out from the TP. During the second degassing process, little to no oil content came out of the tire particles. The samples were collected from the tubes, and BET measurement was conducted. There may have been a small amount of oil on the surface of the TP which resulted in an unsatisfactory correlation coefficient. Further studies are being done to get more reliable BET measurements. In these tests, the samples will be degassed for 5h at 200 °C under a vacuum, and oil-absorbing paper will be used to remove any oil on the TP. Two trials of the untreated and aged TP will be conducted. The amount of each sample will be 500 mg.

3.4.3 Size Distribution of Aged TP

The size distribution of the aged TP was investigated with an optical microscope (Eclipse Ti-E, Nikon Instruments Inc. USA). The microscope was located at Stocker 007, Ohio University. The instrument was operated by Christian Bentum Hammond (Ph.D. student in the civil engineering department, Ohio University). The aged TP were sealed and mounted on the stage of the microscope. Only the finer portions ($<100\ \mu\text{m}$) of the aged TP could fit into our liquid cell since the height of the liquid cell was $\sim 100\ \mu\text{m}$. Thus, using the 100x objective magnification with a limit of $\sim 0.04\ \mu\text{m}$, images of the finer portions of the aged TP were taken and analyzed with MATLAB to obtain their size distribution. Traditional image processing techniques were employed to analyze images obtained from microscopy. Briefly, standard linear filtering was applied to images before objects in images were identified using edge detection image segmentation. Identified image objects were then labeled, and MATLAB's *regionprops* function was used to obtain the structural properties of the objects, such as their area, A. The size of the objects was determined to be $\sim \sqrt{A/\pi}$ and shown in a probability density function (PDF) plot.

Limitations. When the aged TP were sealed to put on the stage of the microscope, only the finer portion of the aged TP could be measured. The coarser particles could not be sealed. The size distribution from the microscope did not include the whole range of the aged TP.

3.4.4 Zeta Potential

The zeta potential of the aged TP was analyzed by Zetasizer Nano ZS. The machine was located at ARC 251, Ohio University. The machine belonged to the Center for Advanced Material Processing at Ohio University. The refractive index and absorption coefficient used were 1.51 (McPherson & Cummings, 1935) and 0.9 (*Zetasizer User Manual* 2008), respectively. The refractive index 1.51 was reported for rubber (McPherson & Cummings, 1935). The absorption value of 0.9 was suggested for blue/black samples (*Zetasizer User Manual* 2008). To calculate the point of zero charge of the aged TP, the aged TP were put into water with pH values 2,3,4,5 and 6. Two samples of aged TP were prepared at each pH value, and zeta potential was measured. The aged TP needed to be in suspension in a liquid for zeta potential measurement. To keep the aged TP in suspension, the aged TP were agitated in orbital shakers for 3 hours at 150 rpm to mix with DI water. After mixing, the aged TP were transferred to a capillary tube for measurement. The concentration of aged TP in the capillary tube was such that the mean count rate was greater than 100000 counts per second. When the mean count rate is less than 100000 counts per second, the concentration of the sample is considered low for zeta potential measurement. The concentration of the sample was also not high enough that it can reduce the scattered light which was being detected by the machine. The samples were kept optically clear for zeta potential measurement.

The adsorption experiments were conducted at pH 6.2. The zeta potential of the aged TP was measured at pH 6.2 before adsorption. To investigate if the zeta potential of the aged TP changes after adsorption, the zeta potential of the aged TP was measured

after adsorption. The samples chosen for zeta potential measurement after adsorption were the ones with an initial heavy metal concentration of 5 mg/L. When measuring the zeta potential of samples after adsorption, the aged TP were already in suspension from the shaking from the adsorption experiment. The suspended aged TP in liquid were transferred to a capillary tube for measurement. The concentration was not high or low to obstruct zeta potential measurement. In other words, the concentration of the sample in the capillary tube was such that the mean count rate was greater than 100000 counts per second, and the samples were optically clear. Two samples for each criterion were measured to ensure reproducibility.

Limitations. The Zetasizer machine can only measure the surface charge of the particles suspended in the liquid. The TP used in this study had a wide range of sizes. The finer portion of the sample TP was in suspension in the liquid, and the coarser portion settled in the capillary tube. Zetasizer could only measure the surface charge of the finer portion of the TP sample.

3.4.5 Fourier-Transform Infrared Spectroscopy (FT-IR)

Untreated TP, aged TP, lead-adsorbed aged TP, and copper-adsorbed aged TP were analyzed by FT-IR. The lead-adsorbed aged TP and copper-adsorbed aged TP were obtained after the single batch adsorption tests. The adsorbent dose for lead and copper tests was 25 and 200 mg, respectively. The initial concentration of the heavy metals was 5 mg/L. After the adsorption test, the lead and copper adsorbed aged TP were vacuum filtered and oven dried at 100° C for 24 h. Untreated TP, aged TP, lead-adsorbed aged TP, and copper-adsorbed TP were collected in sealed tubes and delivered to the Institute

for Sustainable Energy and the Environment at Ohio University for the FT-IR analysis. Each sample was 10 mg. Chiderah Jessica Chukwuka, one of the Ph.D. students from Dr. Damilola Daramola's group, operated the machine (Nicolet 6700 spectrometer). The attenuated total reflectance method was used. At first, the background spectra were calculated. The TP were put on top of the spectrometer, and the clamps were tightened. The TP were held in proximity to the crystal, and infrared light was bounced off the sample. The FT-IR spectra of the sample were generated after subtracting the background spectra. The TP were analyzed in the range of 4000-500 cm^{-1} . The FT-IR spectra was run through the library to identify the material. After the material was identified, the positions of the absorbance peaks were compared to identify the functional groups in the sample.

3.4.6 X-ray Photoelectron Spectroscopy (XPS)

XPS analysis was performed on aged TP and lead-adsorbed aged TP. Since the copper adsorption on aged TP was below the XPS instrument detection limit, copper-adsorbed aged TP were not analyzed. The initial concentration of lead was 1000 mg/L for the adsorption test. The initial concentration was chosen to be high due to the sensitivity of the XPS machine. 5g of aged TP was used in 50 mL lead solution. The sample was shaken in an orbital shaker at 150 rpm for 48 h. After the elapsed time, the samples were centrifuged at 4000 rpm for 15 mins. The lead-adsorbed aged TP were vacuum filtered. The lead adsorbed aged TP were oven dried at 100° C for 24 h. The dried sample was stored in a sealed tube. The aged TP before adsorption and lead adsorbed aged TP were sent to the Materials Characterization Facilities at West Virginia University in sealed tubes. The weight of each sample was 1 g. The XPS analysis was done by Dr. Qiang

Wang. The XPS machine model was Physical Electronics VersaProbe 5000. The samples were mounted on the sample holder and put in the XPS machine chamber. An alignment gauge was used to properly align the sample holder before closing the chamber. The x-ray beam in the machine excites the electrons in the sample, and the energy analyzer measures the speed of the electron leaving the sample to measure the binding energy. The XPS x-ray source was focused aluminum K- α 1, and the x-ray was set at 100 um/25W/15kV. The system pressure was 2×10^{-6} Pa, and the neutralizer was on during the experiment. A survey scan showing peaks of different elements present on the surface was produced by analysis. A high-resolution scan of the elemental peaks was done to analyze the bonds present and to quantify the intensity of each bond.

Chapter 4: Results and Discussion

4.1 Morphology, Surface Area, and Size Distribution

The SEM images of untreated and aged TP are shown in Figure 9. The shapes of the TP were irregular. There was a presence of fabric and textile fragments in untreated TP (Figure 9A). The BET surface area (S_{BET}) for untreated and aged TP was found to be 0.15 and 0.28 m^2/g . The TP size ranged from 1 μm (Appendix C) to many hundreds of micrometers (SEM images).

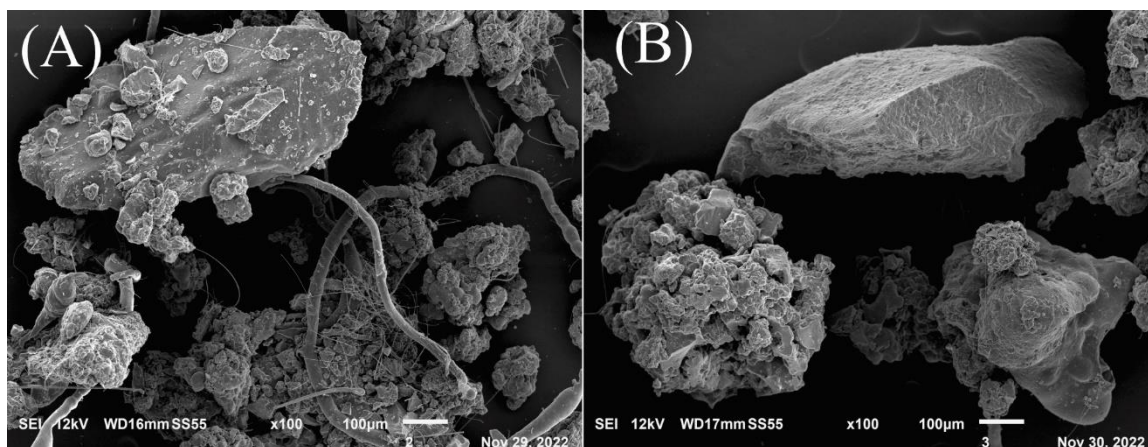


Figure 9. SEM images of (A) untreated (B) aged TP.

4.1.1 Discussion

There was a presence of textile fragments in untreated TP image (Figure 9A). Textiles are used in tires for reinforcement and stability. There were no textile fragments in aged TP image (Figure 9 B). Both the untreated and aged TP seemed nonporous from the SEM images (Figure 9). Aging with 30% HNO_3 may have removed the textile, but the morphology of untreated and treated TP were comparable from the SEM images.

The size range of the TP used in this study was wide. The size ranged from $1\mu\text{m}$ (Appendix C) to many hundreds of micrometers (SEM images). In order to simulate the wide range of TP involved in the adsorption-desorption process of heavy metals in nature, a wide size range of TP was used in this study.

In comparison to untreated TP ($0.15\text{ m}^2/\text{g}$), the aged TP had a higher BET surface area ($0.28\text{ m}^2/\text{g}$). Aging might have changed the surface and pore structure to increase the S_{BET} . The limitations of the BET measurements were discussed in the methodology section. In appendix A, the N_2 adsorption-desorption isotherm and correlation coefficient curves, and pore distribution reports from BET surface area measurement of untreated and aged TP are shown.

4.2 Zeta Potential

The pH_{pzc} of the aged TP was found to be pH 2 by measuring zeta potential at different pH values (Figure 10).

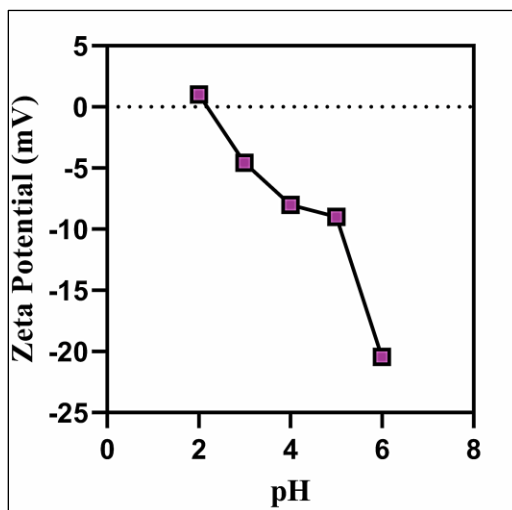


Figure 10. Zeta potential of aged TP at different pH values.

The pH of the heavy metal solution for batch adsorption tests was 6.2. Table 7 shows the zeta potential and pH of aged TP before and after heavy metal adsorption. During batch adsorption tests, the samples with an initial metal concentration of 5 mg/L were used to measure the final pH and zeta potential after adsorption.

Heavy Metal	ZP before adsorption	Initial pH	ZP after adsorption	Final pH
Pb	-20.43 mV	6.2	-18.5 mv	6.2
Cu	-20.43 mV	6.2	-19.9 mV	4

Table 7. Zeta potential and pH of aged TP before and after heavy metal adsorption.

The zeta potential of the aged TP hardly changed after heavy metal adsorption compared to the initial value. There was a slightly greater change in zeta potential for lead after adsorption than copper. There was no pH change in lead solution before and after adsorption. For copper adsorption on aged TP, the initial pH of 6.2 of the copper solution before adsorption changed to pH 4 after adsorption.

4.2.1 Discussion

The pH_{pzc} of the aged TP was pH 2. That means, the surface of the TP was negatively charged above pH 2 and positively charged below it. At experimental pH conditions (pH 6.2), the aged TP were negatively charged. Hence, electrostatic attraction

was a possible mechanism for the adsorption of positively charged metal ions on negatively charged TP.

When an object is exposed to a fluid, a structure known as electric double layer (EDL) develops on the object's surface. EDL has a Stern layer closer to the adsorbent surface and a diffuse layer on top of the Stern layer. The Stern layer consists of ions that chemically interact with the surface charge of the object. The diffuse layer consists of ions that move in the fluid and are loosely bound by electric attraction. Zeta potential is the surface charge property built up at the interface of EDL. While the adsorption of ions on the diffuse layer occurs by electrostatic attraction, chemical bonding is required for adsorption on the Stern layer between the TP and the metal ions (Shahrokhi-Shahraki et al., 2021) (Wakatsuki et al., 1974). Adsorption of ions on the Stern layer changes zeta potential because of the formation of chemical bonds (R. Xu et al., 2011). For the adsorption on the diffuse layer, the zeta potential does not change. The zeta potential of the aged TP hardly changed after heavy metal adsorption compared to the initial value. The change in zeta potential after adsorption for lead was a little higher than the change for copper. The comparable zeta potential after adsorption indicated electrostatic attraction was a possible mechanism. Lead had a slightly larger change in zeta potential following adsorption than copper, indicating that the possibility of bonding on Stern layer was higher for lead.

The pH value of the copper solution changed after adsorption on aged TP. There was no change for lead. The initial pH before the adsorption for both lead and copper was 6.2. At pH 6.2, the copper species present are Cu^{2+} and $\text{Cu}(\text{OH})^+$ (Figure 6 B). At pH 6.2,

the lead species present are Pb^{2+} and $\text{Pb}(\text{OH})^+$ (Figure 6 A). It was unclear why the pH of copper changed after adsorption. Further testing on the distribution of the species of lead and copper as function of pH for the experimental conditions might help explain the pH drop of copper after adsorption.

4.3 FT-IR Results

An infrared spectrum of an object's absorption/emission can be obtained using the FTIR. High-resolution spectral data are concurrently collected over a broad spectral range by an FTIR spectrometer. The raw data must be transformed using the Fourier transform to produce the real spectrum. Measurement of the amount of light a sample absorbs at each wavelength is the aim of FT-IR. A variety of functional groups can be detected using the rapid, non-destructive, and time-saving FT-IR technique, which is also sensitive to changes in molecular structure. On the basis of the chemical composition and physical state of the entire sample, FTIR provides information (Cocchi et al., 2004).

Figure 11 (A-B) shows the FT-IR spectra for untreated TP, aged TP, lead-adsorbed aged TP, and copper-adsorbed aged TP.

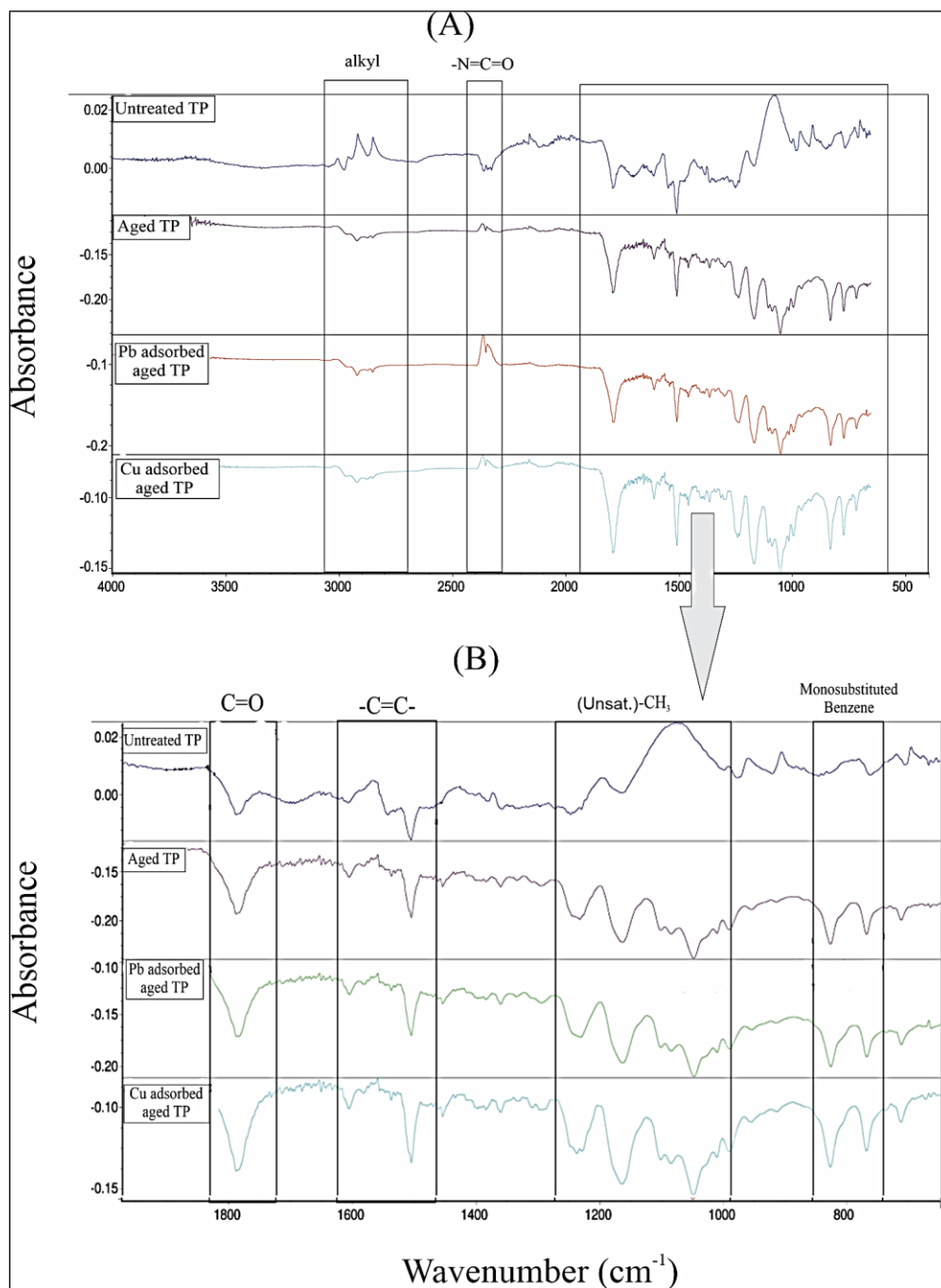


Figure 11.(A-B) FT-IR spectra for Untreated TP, aged TP, lead adsorbed aged TP (initial concentration 5mg/L), and copper adsorbed aged TP (initial concentration 5mg/L).

The peaks at 3000-2800 cm^{-1} were represented by $-\text{CH}_3$ (aliphatic) stretching vibrations. (HUCZYNSKI et al., 2011) (Smith, 2022). The peak at 2350-2250 cm^{-1} attributed to the functional group $-\text{N}=\text{C}=\text{O}$ (isocyanate) (HUCZYNSKI et al., 2011). The $\text{C}=\text{O}$ (carboxylic) groups were identified at 1780-1770 cm^{-1} , and the aromatic $\text{C}=\text{C}$ stretching vibration at 1510-1500 cm^{-1} (HUCZYNSKI et al., 2011). The band at 1250-1000 cm^{-1} was (Unsaturated)- CH_3 rocking vibration, and monosubstituted benzene group was identified at 820-720 cm^{-1} (HUCZYNSKI et al., 2011).

4.3.1 Discussion

The $-\text{CH}_3$ aliphatic group peak (3000-2800 cm^{-1}) was highest for untreated TP (Figure 11 A). The aging process might have attributed to the reduction of the intensity of the group. After lead and copper adsorption on aged TP, a shift in intensity (stronger/weaker) or a shift of bands to a new position was seen in FT-IR spectra compared to that of aged TP before adsorption (Figure 12). Hotová et al. (2020) suggested that oxygen containing groups and/or aromatic π -electrons are involved in the surface complexation of heavy metals. The peak for $-\text{N}=\text{C}=\text{O}$ (2350-2250 cm^{-1}) was highest in lead-adsorbed aged TP compared to that of aged TP and copper-adsorbed aged TP (Figure 12). For $\text{C}=\text{O}$ (1780-1770 cm^{-1}) groups, there was a shift in intensity for copper-adsorbed aged TP compared to aged TP and lead-adsorbed aged TP (Figure 12). The shift in intensity (stronger/weaker) of oxygen containing and aromatic π -electron containing groups indicated their involvement in surface complexation with heavy metals.

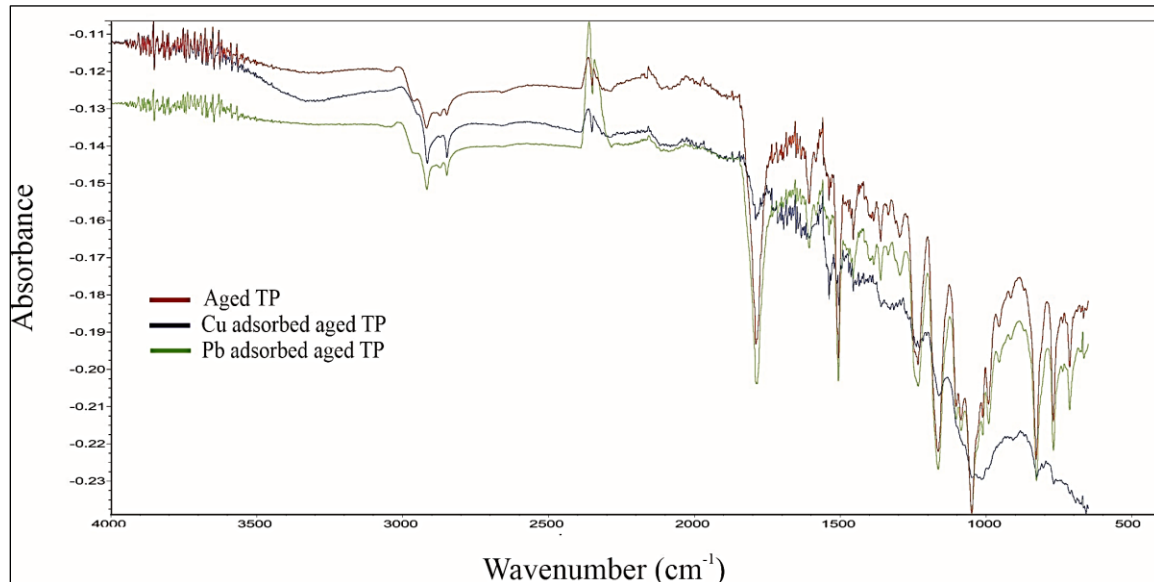


Figure 12. Comparison of FT-IR spectra of aged TP before and after heavy metal adsorption.

4.4 XPS Results

XPS can identify the elements present in the elemental composition of the material which are present on the surface or within the material. XPS is a quantitative spectroscopic method that can also identify the chemical state and electronic structure of the elements present on the surface or within the material.

To determine the impact of functional groups on the surface complexation with heavy metals, XPS spectra of aged TP was analyzed before and after lead adsorption. Copper adsorbed aged TP was not examined since the adsorption was below the XPS instrument detection limit. There was no lead peak on the aged TP XPS spectra before adsorption. The formation of the Pb 4f group at peak 139.08 eV after adsorption indicated the adsorption of lead on aged TP (Figure 13).

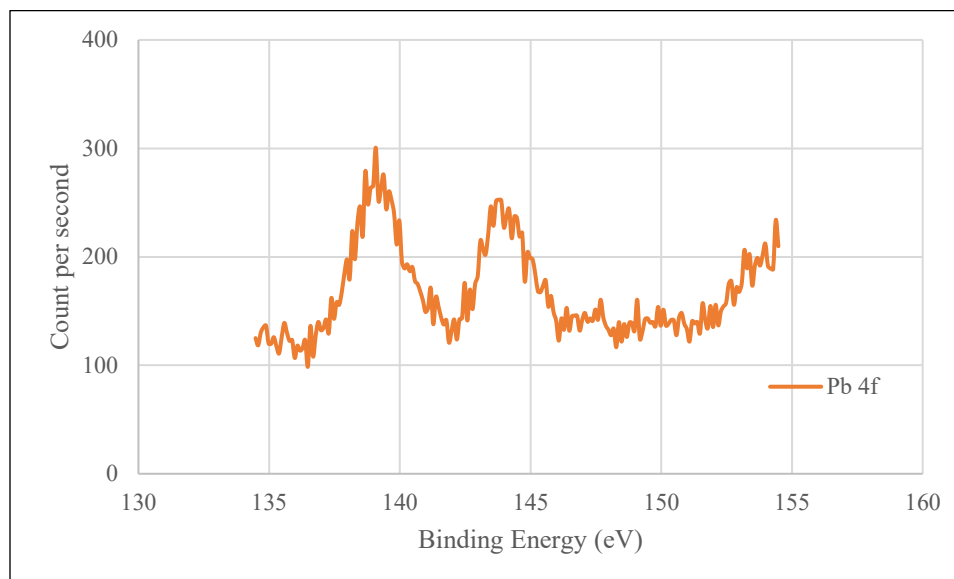


Figure 13. Pb 4f XPS spectra on aged TP after lead adsorption.

Figure 14 (A-B) shows the XPS spectra of C1s before and after lead adsorption. The C1s XPS spectra showed four peaks with binding energy 284.845 eV (C-C/C-H), 286.345 eV (C=O), 288.095 eV (C-O), and 282.745 eV (inorganic carbon) (Shahrokhi-Shahraki et al., 2021) (Wu et al., 2019).

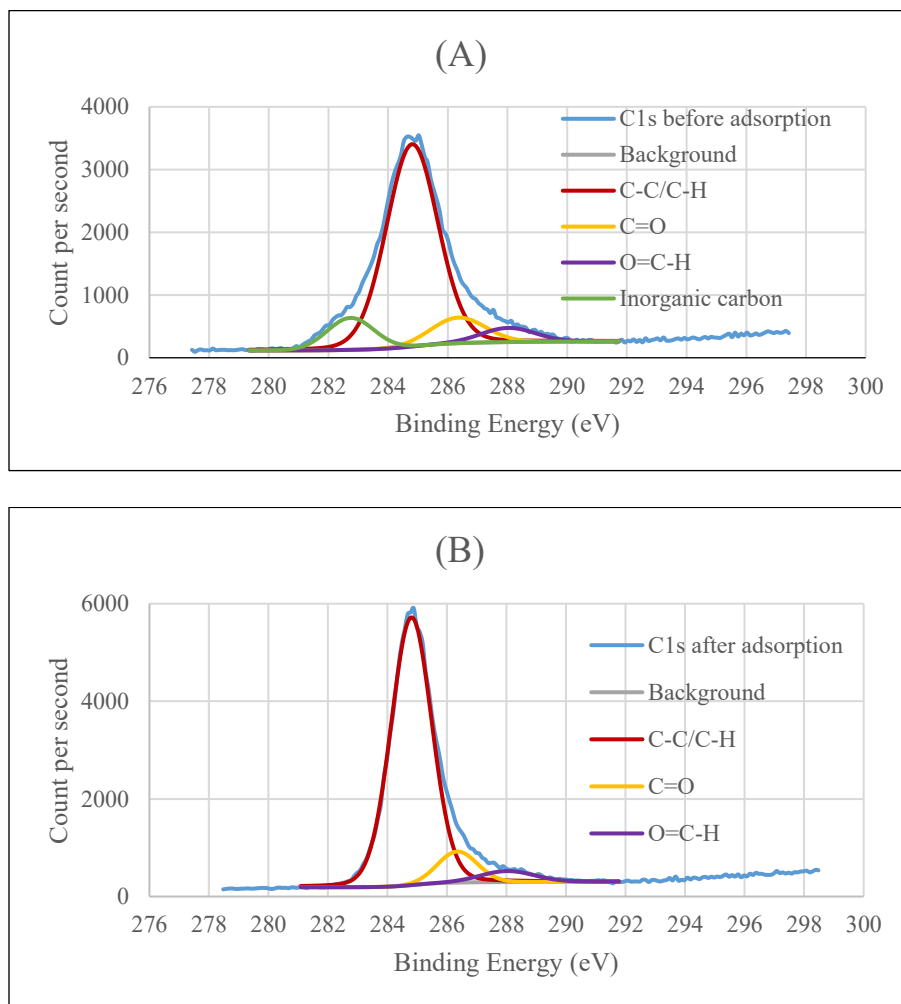


Figure 14. XPS spectra of C1s (A) before and (B) after lead adsorption on aged TP.

Figure 15 (A-B) shows the XPS spectra of O1s before and after lead adsorption. For O 1s spectra, two peaks with binding energy 531.645 eV (C-O) and 533.045 eV (O-C=O) were observed (Guo et al., 2018).

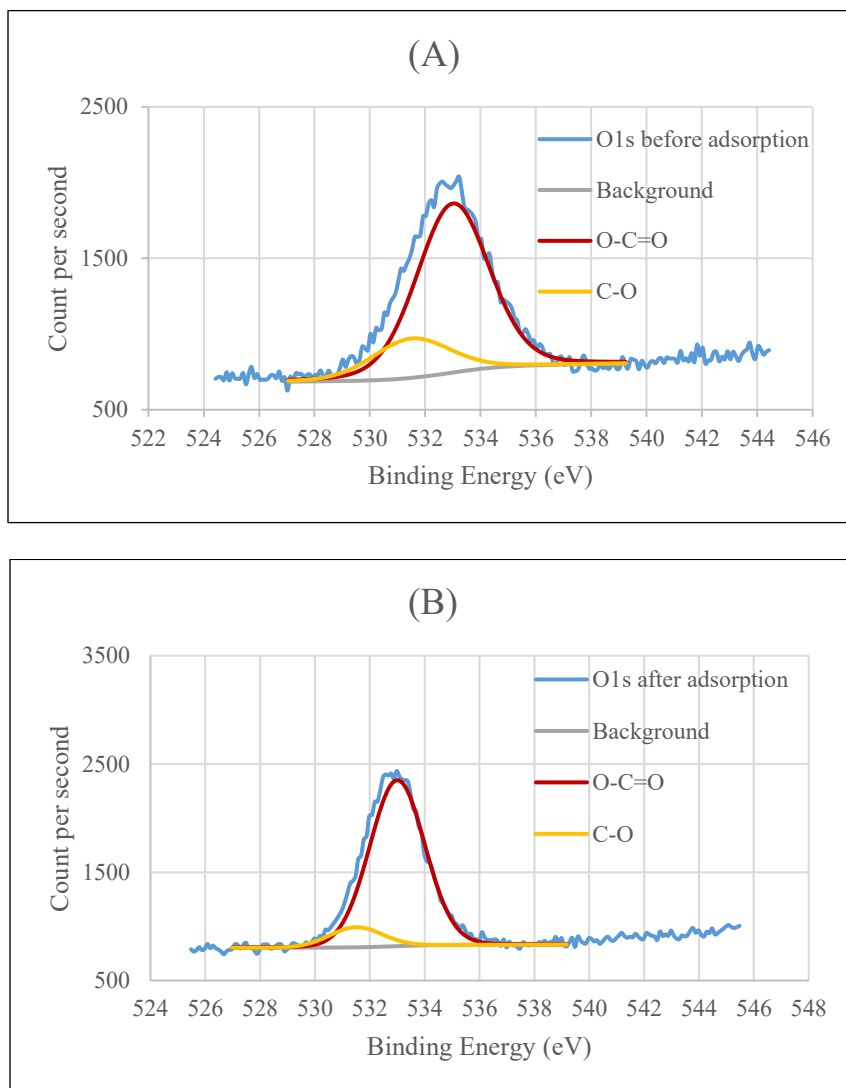


Figure 15. XPS spectra of O1s (A) before and (B) after lead adsorption on aged TP

4.4.1 Discussion

For C 1s XPS spectra, there was no inorganic carbon after adsorption (Figure 14B). This may be attributed to the contribution of sorption to carbon black, which could stem from tar-like liquid phases of the carbon black and form a metal-inorganic-organic

carbon complex. After Pb adsorption, there was no shift in the binding energy of the functional groups. However, there was a change in the relative content of the functional groups. For O 1s XPS spectra, there was an increase in the carboxylic acid (O-C=O) group after adsorption. The relative content of (O-C=O) group increased from 80.34 to 89.73% (Figure 16). The (C-O) group decreased from 19.66 to 10.27% after adsorption (Figure 16). In C1s spectra, (C-C/C-H) changed from 74.72 to 85.74% (Figure 16).

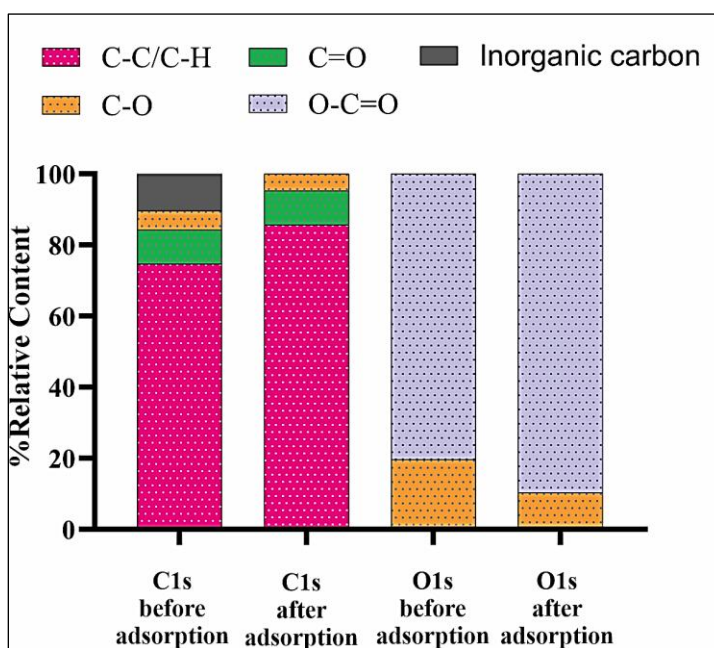


Figure 16. Relative contents of the functional groups in C1s and O1s XPS spectra before and after adsorption.

As a result of lead adsorption, the content of the C-O group decreased, whereas the O-C=O group increased. This can be attributed to the formation of $\text{Pb}^{2+}\text{-O-C=O}$ or Pb-O functional groups on the surface of aged TP (Shahrokhi-Shahraki et al., 2021) (Guo et al.,

2018). Hence, surface complexation was a possible adsorption mechanism in heavy metal adsorption on aged TP.

4.5 Single Batch Adsorption Results

The adsorption data were fit into Langmuir and Freundlich isotherm models to examine the adsorption behavior. Each test was conducted twice to ensure reproducibility and the average was used for analysis. To get a robust adsorption curve, screening tests were conducted to choose an adsorbent dose (Appendix B). The chosen adsorbent doses were 25 mg and 200 mg in 50mL lead and copper solutions respectively. Figure 17 (A-B) shows single adsorption isotherm curves for lead with untreated and aged TP. The equilibrium adsorbent-phase concentration (q_e) increased with increasing equilibrium concentration of heavy metals in solution (C_e).

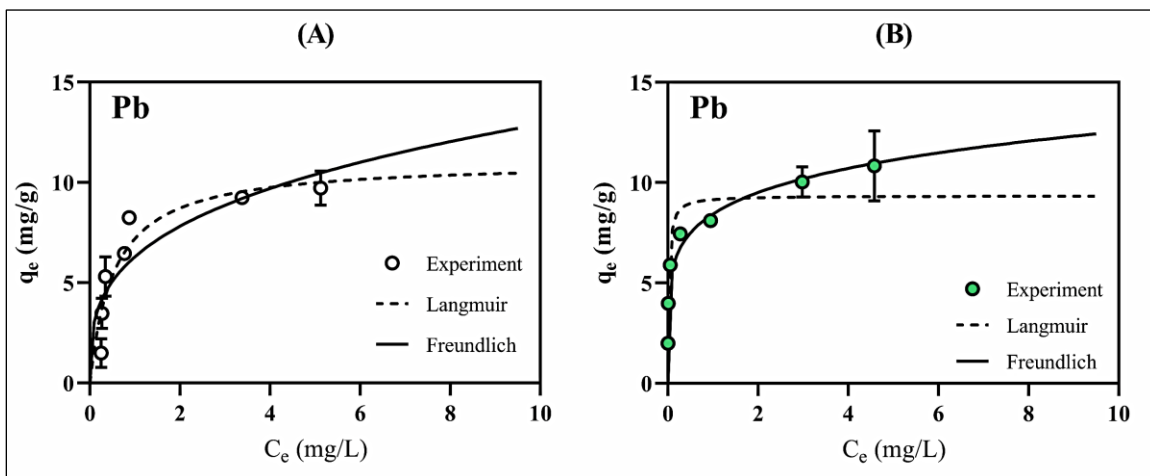


Figure 17. Adsorption isotherm of lead for (A) untreated TP and (B) aged TP.

The Langmuir model is valid when there is a fixed number of sites in the adsorbent where adsorbate molecules can be bound. The Langmuir model assumes reversible chemical equilibrium between the adsorbent surface and adsorbate solution. The Langmuir model assumes a homogeneous surface for adsorbent and accumulation of adsorbate in only a single layer. On the other hand, the Freundlich model is valid when there are multiple layers of adsorbate bound to the adsorbent. The Freundlich model assumes that the adsorbent has a heterogeneous surface. Fan et al. (2021) and Sivaraman et al.(2022) reported the Freundlich curve was the better fit for heavy metal adsorption on TP. Heavy metal adsorption on microplastics followed both the Langmuir (Godoy et al., 2019) (Wang et al., 2020) and Freundlich models (Mao et al., 2020).

Nonlinear regression was used to determine the model parameters and root mean square error (RMSE). The isotherm parameters and RMSE values are listed in Table 8.

Heavy metal	Adsorbent	Langmuir			Freundlich		
		Q_m (mg/g)	b_a (L/mg)	RMSE	K_f $\frac{\text{mg/g}}{(\text{mg/L})^{1/n}}$	1/n	RMSE
Pb	Untreated	11.054	0.537	1.021	6.288	0.312	1.402
	TP						
	Aged TP	9.342	0.021	0.980	8.433	0.172	0.665
Cu	Untreated	0.753	0.101	0.087	0.614	0.150	0.031
	TP						
	Aged TP	0.575	0.007	0.071	0.517	0.132	0.023

Table 8. Langmuir and Freundlich parameters for Pb and Cu adsorption on TP.

Figure 18 (A-B) shows single adsorption curves for copper with untreated and aged TP. The equilibrium adsorbent-phase concentration (q_e) increased with increasing equilibrium concentration of heavy metals in solution (C_e).

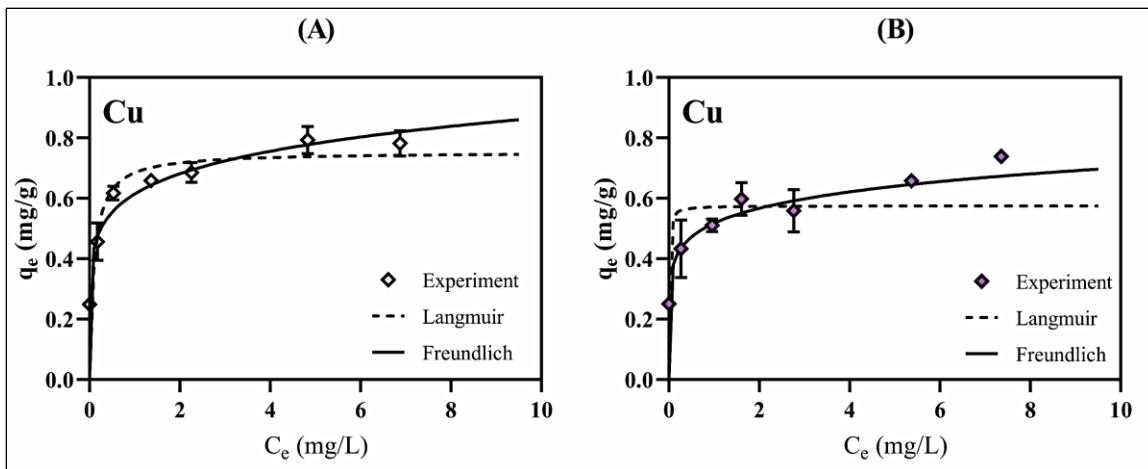


Figure 18. Adsorption isotherm of copper for (A) untreated TP and (B) aged TP.

4.5.1 Discussion

Although the BET surface area of untreated and aged TP were different, the adsorption data for lead with untreated and aged TP were comparable (Figure 17). It indicated that the surface area did not play a significant role in the adsorption of lead on TP. The maximum adsorption capacity (Q_m) for lead with untreated and aged TP was 11.054 and 9.342 mg/g, respectively (Table 8). On the other hand, the adsorption capacity parameter (K_f) for lead from the Freundlich model was 6.288 and 8.433 (mg/g)/(mg/L)^{1/n} for untreated and aged TP, respectively (Table 8). The capacity parameters from the Langmuir and the Freundlich models for lead were much higher than those of any microplastics (Table 2). The model parameters for lead were lower than those of typical

adsorbents (Table 3). The Freundlich coefficient $1/n$ was less than 1 (0.312 for untreated and 0.172 for aged TP) for lead, which indicated that adsorption on TP followed a non-linear pattern (Table 8). For adsorption of lead on untreated TP, the RMSE (1.021) was lower for the Langmuir model than the RMSE (1.402) for the Freundlich model. For aged TP, the RMSE (0.665) was lower for the Freundlich model than the RMSE (0.980) from the Langmuir model. RMSE values indicated the Langmuir model was the better fit for lead adsorption on untreated TP, whereas the Freundlich model was the better fit for lead adsorption on aged TP. This finding potentially indicated that monolayer adsorption occurred for untreated TP and aging caused heterogeneity to the TP surface resulting in multilayer adsorption.

The adsorption data for untreated and aged TP are comparable for copper (Figure 18). This indicated that surface area of TP did not play a significant role in copper adsorption. The same applied to lead adsorption on TP. The maximum adsorption capacity (Q_m) for copper with untreated and aged TP was 0.753 and 0.575 mg/g, respectively (Table 8). The adsorption capacity parameter (K_f) for copper from the Freundlich model was 0.614 and 0.517 (mg/g) / (mg/L)^{1/n} for untreated and aged TP respectively (Table 8). The capacity parameters for copper were much higher than those of any microplastics (Table 2) and lower than those of any typical adsorbents (Table 3). The Freundlich coefficients $1/n$ (0.150 for untreated and 0.130 for aged TP) for copper adsorption on TP were less than 1, which indicates adsorption did not follow a linear pattern. For the adsorption of copper on untreated TP, the RMSE (0.031) from the Freundlich model was lower than the RMSE (0.087) from the Langmuir model.

Similarly, for aged TP, the RMSE (0.023) from the Freundlich model was lower than the RMSE (0.071) from the Langmuir model. Hence, the Freundlich model was the better fit for copper adsorption on both untreated and aged TP.

Compared to lead, the copper adsorption on TP was very low. Higher adsorption of lead compared to copper was also reported for tire-derived activated carbon (Shahrokhi-Shahraki et al., 2021) and microplastics (Godoy et al., 2019). This finding may be explained by the properties of the metals, such as the hydrolysis constant, electronegativity, and the hydration radius. A higher hydrolysis constant means a larger portion of the ion has hydrolyzed. With a higher hydrolysis constant of heavy metals, the affinity for adsorption increases. However, specific adsorption of the metal ions decreases. The hydrolysis constant for lead is higher than that of copper (Table 4). Hence, the lead ions have a greater affinity for adsorption than copper ions. The electronegativity of Pb^{2+} (2.33) is greater than that of Cu^{2+} (1.90). The affinity of accepting electrons for lead is higher than copper. Hence, lead has an advantage over copper for adsorption through surface complexation. The hydrated radius of Pb^{2+} (4.01 Å) is smaller than that of Cu^{2+} (4.19 Å). Due to the smaller size, lead ions have the advantage over copper ions for adsorption sites.

Figure 17 and Figure 18 show that the Langmuir and the Freundlich models were under and over predicting the data. Hence, both the Langmuir and the Freundlich models were not best for describing adsorption of lead and copper on TP. TP are composite adsorbents. They are made up of rubber, SBR, carbon black etc. Sorption on TP might be a combination of different processes. The adsorption on polymer, rubber, and carbon

black may follow different mechanisms. Therefore, a more complex model might better describe the adsorption of lead and copper on TP.

Microplastics are considered vectors for heavy metals and organic compounds. However, some argue that particulate matter, which is present in far greater quantities in natural water, outcompetes microplastics as sorbents (Koelmans et al., 2016). The adsorption capacity of microplastics are higher than particulate matter for heavy metals (Koelmans et al., 2016). The adsorption capacity of the TP was higher than for microplastics for heavy metals in this study. Particulate matter is more prevalent than microplastics and TP in nature. To be certain that the TP are strong enough adsorbents to alter the bioavailability and toxicity of heavy metals, more research is required.

4.6 Competitive Adsorption Results

The competitive adsorption tests were conducted in a binary-solute (Pb, Cu) system. The competitive adsorption data were fit into the Langmuir and Freundlich models. For competitive adsorption, the concentration of lead and copper was kept the same in the samples. The adsorbent dose was 25 and 200 mg aged TP for 50mL heavy metal solution. That means, in the mixed solution, lead adsorption was analyzed when the adsorbent dose was 25mg. When the adsorbent dose was 200 mg, copper adsorption was analyzed in the competitive adsorption test. Figure 19 (A) shows the competitive adsorption isotherms for lead. The q_e increased at first and balanced out afterward. Figure 19 (B) compares competitive lead adsorption isotherm to single adsorption isotherm.

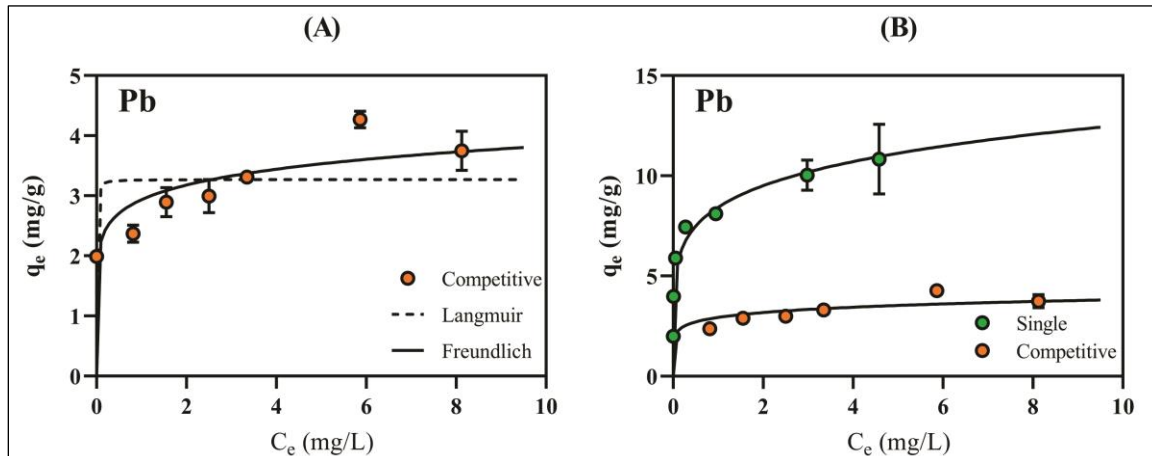


Figure 19. (A) Competitive adsorption isotherm for lead with aged TP. (B) Comparison of single and competitive adsorption isotherm for lead with aged TP.

Nonlinear regression was used to determine the model parameters and root mean square error (RMSE). The isotherm parameters and RMSE values are listed in Table 9.

Heavy metal	Adsorbent	Langmuir			Freundlich		
		Q_m (mg/g)	b_a (L/mg)	RMSE	K_f $\frac{\text{mg/g}}{(\text{mg/L})^{1/n}}$	$1/n$	RMSE
Pb	Aged TP	3.271	0.003	0.565	2.933	0.115	0.372
Cu	Aged TP	0.253	0.200	0.058	0.179	0.215	0.048

Table 9. Langmuir & Freundlich parameters for competitive adsorption.

Figure 20 (A) shows the adsorption of copper on aged TP in a binary-metal system. Figure 20 (B) compares competitive copper adsorption isotherm to single adsorption isotherm.

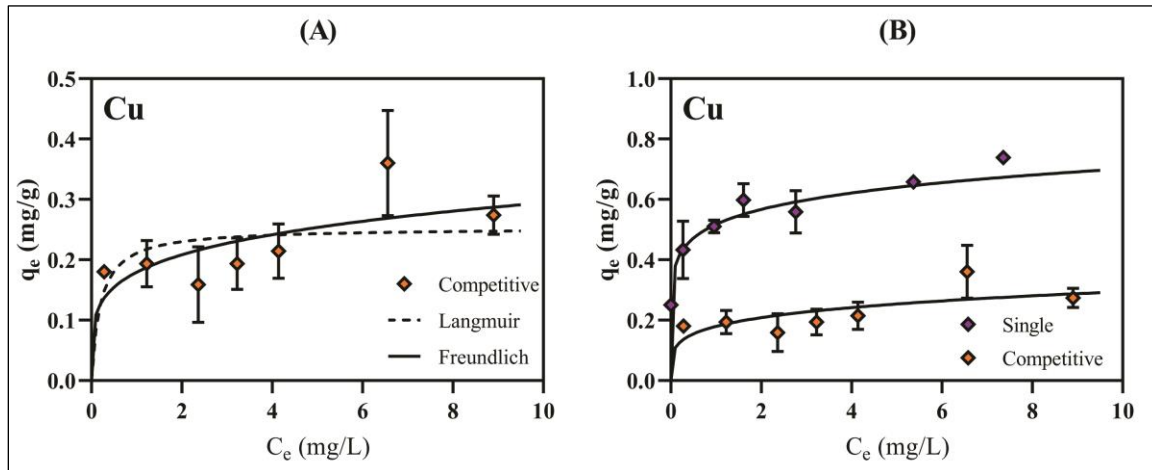


Figure 20. (A) Competitive adsorption isotherm for copper with aged TP.

(B) Comparison of single and competitive adsorption isotherm for copper with aged TP.

4.6.1 Discussion

The adsorption capacity of aged TP in binary-metal system decreased compared to the single metal system for lead (Figure 19B). This can be attributed to the coexistence of copper ions. The maximum adsorption capacity (Q_m) and the Freundlich adsorption capacity parameter (K_f) for competitive lead adsorption on aged TP were 3.271 mg/g and 2.993 (mg/g)/(mg/L)^{1/n}, respectively (Table 9). The RMSE (0.372) from the Freundlich model was lower than the RMSE (0.565) from the Langmuir model, which indicated the Freundlich model was the better fit. $1/n$ value (0.115) from the Freundlich model was less than 1, which indicated the nonlinearity of the curve.

The copper adsorption was inhibited by the coexisting lead ions (Figure 20B). The maximum adsorption capacity (Q_m) and the Freundlich adsorption capacity parameter (K_f) for competitive copper adsorption on aged TP were 0.253 mg/g and 0.179

$(\text{mg/g})/(\text{mg/L})^{1/n}$, respectively (Table 9). The RMSE (0.048) from the Freundlich model was lower than the RMSE (0.058) from the Langmuir model. Hence, the Freundlich model was the better fit. The adsorption was not linear, as indicated by the Freundlich coefficient $1/n$ (0.215), which was less than 1.

Figure 21 (A) compares maximum adsorption capacity (Q_m) in single and competitive adsorption for heavy metal. The Q_m was reduced by 64.98% for lead and 56% for copper. This indicates inhibition by copper was greater than that by lead.

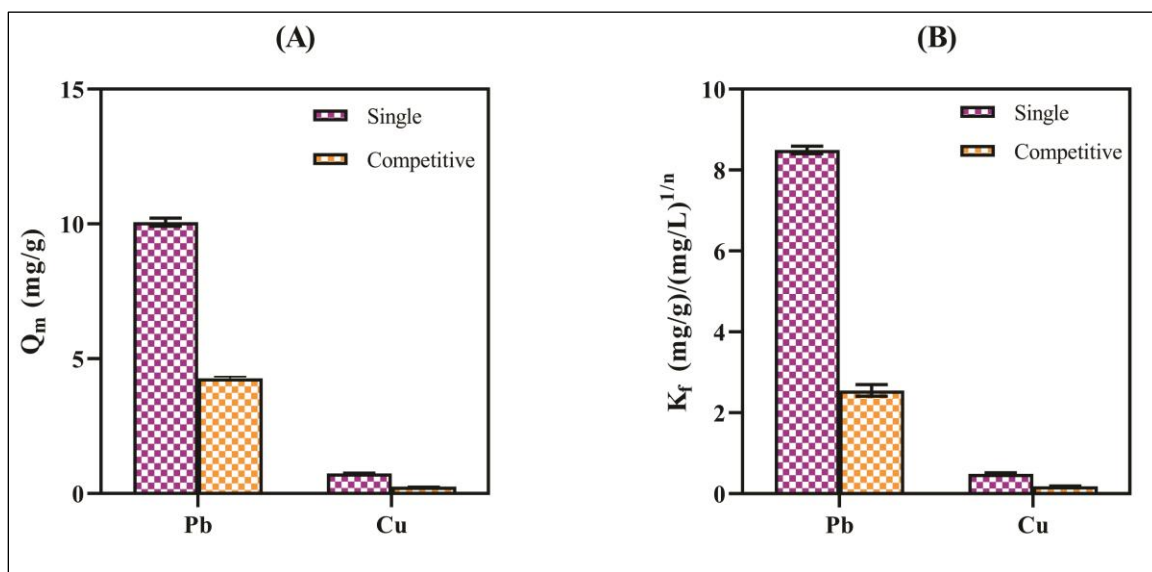


Figure 21. (A) Comparison of maximum adsorption capacity (Q_m) from the Langmuir model for single and competitive adsorption isotherms for lead and copper. (B) Comparison of maximum adsorption capacity parameter (K_f) from Freundlich model for single and competitive adsorption isotherms for lead and copper.

Figure 21 (B) compares the Freundlich capacity parameter (K_f) in single and competitive adsorption for copper. The K_f was reduced by 65.22% and 65.37% for lead and copper, respectively. The K_f reduction values indicated that the inhibition by lead and copper were comparable for K_f . Figure 19 (A) and Figure 20(A) show that the adsorption of lead was higher than copper on aged TP in a binary-metal system. Like single metal system, aged TP selects lead over copper in competitive adsorption.

4.7 Effect of pH on Adsorption

Figure 22 (A-B) shows strong pH dependence of lead and copper adsorption on TP. Figure 22 (A) shows the effect of pH on lead adsorption on aged TP in terms of q_e . Figure 23 (A) shows the change in removal efficiency (%) of lead by aged TP with changing pH.

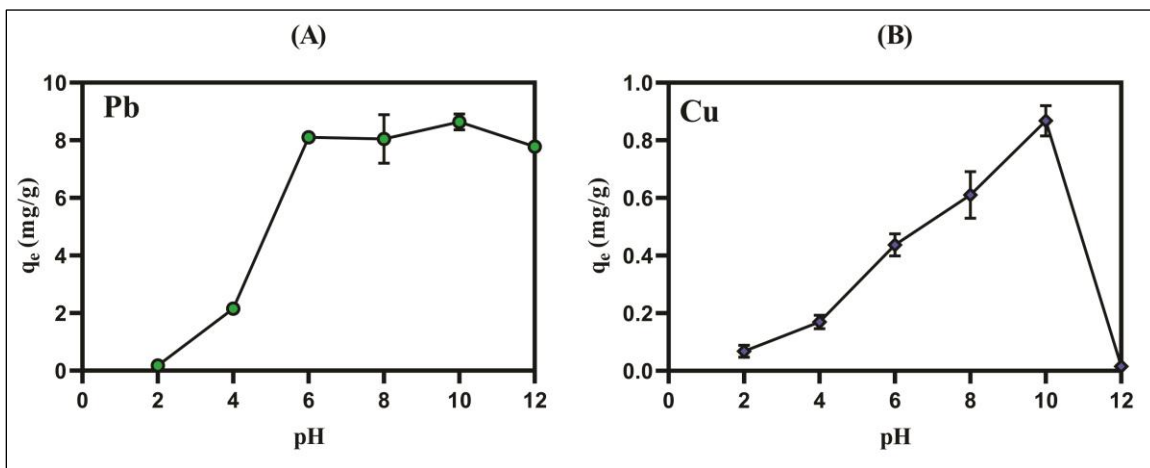


Figure 22. Effect of pH on (A) Pb^{2+} and (B) Cu^{2+} adsorption on aged TP at initial concentration 5mg/L.

At pH 2-6, lead adsorption gradually increased. At pH 6-12, the lead adsorption did not change notably. In terms of removal efficiency, the lead removal (1.77%) was lowest at pH 2 and reached maximum of 86.35% at pH 10. The lead removal efficiency at pH 6-12 was comparable.

Figure 22 (B) shows the effect of pH on copper adsorption on aged TP, and copper removal (%) by aged TP is shown in Figure 23 (B). There was a gradual increase in copper adsorption from pH 2-10. The adsorption abruptly went down at pH 12. The maximum copper removal was at pH 10.

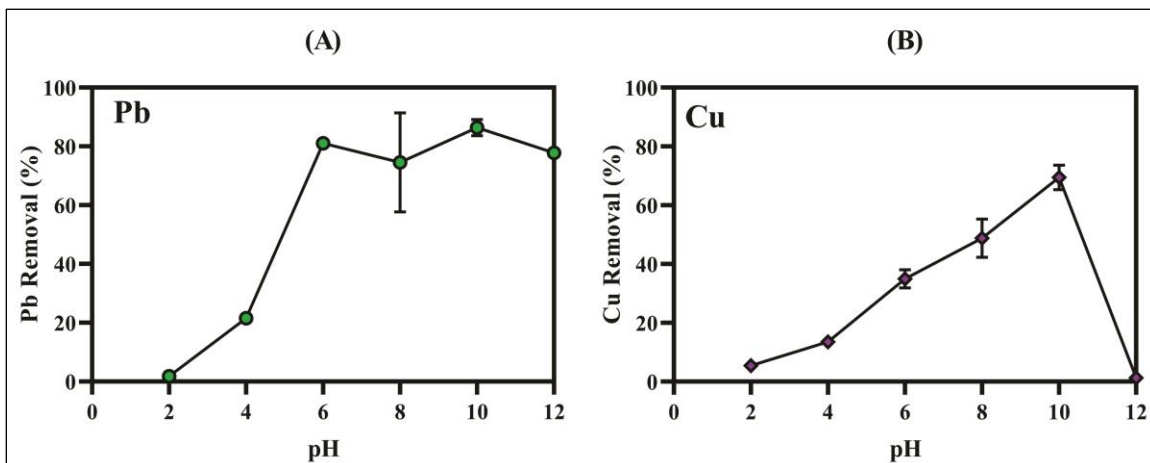


Figure 23. Effect of pH on (A) Pb^{2+} and (B) Cu^{2+} removal efficiency of aged TP at initial concentration 5mg/L.

4.7.1 Discussion

Lead and copper adsorption on aged TP was strongly pH-dependent, as shown in Figure 22(A-B). Strong pH dependence suggests that surface complexation plays a major

role in adsorption (Bradbury & Baeyens, 2002) (Um & Papelis, 2003) (D. Xu et al., 2008).

At $\text{pH} \leq 7.5$, the predominant lead species in the aqueous system was Pb^{2+} (Figure 6A). Hence, the positively charged lead ions were attracted to negatively charged TP. However, the lead removal at pH 2 was close to zero, and at pH 4, it was 21.52%. This can be explained by the zeta potential of TP. At pH 2, the surface charge of TP was zero (Figure 10), which explained the close-to-zero lead adsorption. The zeta potential of TP at pH 4 and 6 were -8.02 and -20.43 mV, respectively. Since the surface charge of TP at pH 4 was much lower than that at pH 6, the adsorption of lead was lower at pH 4 than at pH 6. At pH 7.5-12, there was coexistence of $\text{Pb}(\text{OH})^+$, $\text{Pb}(\text{OH})_2$ (aq), $\text{Pb}_3(\text{OH})_4^{2+}$ and $\text{Pb}(\text{OH})_3^-$. The presence of these species did not influence the lead adsorption notably. The highest adsorption of lead on aged TP was found at pH 6-12.

In terms of copper removal (%), the removal (1.26%) was lowest at pH 12. The highest removal (69.42%) was achieved at pH 10. At $\text{pH} \leq 7.8$, the dominant copper species present in the aqueous medium was Cu^{2+} (Figure 6B). At $\text{pH} \leq 7.8$, the adsorption was the result of electrostatic attraction between negatively charged TP and positively charged copper ions. At pH 2, the surface charge of TP was zero (Figure 10), which explained the low copper removal (5.45%) at that point. The copper removal was 13.55 and 34.97% at pH 4 and 6, respectively. Since the surface charge of TP was much higher at pH 6 than at pH 4 (Figure 10), the copper removal was higher at pH 6. At pH 8, the major Cu species was $\text{Cu}(\text{OH})^+$ in the aqueous system. The low solubility of $\text{Cu}(\text{OH})^+$ might have contributed to the higher adsorption of copper. The copper removal reached

its highest value (69.42%) at pH 10. At pH 10, the dominant species was $\text{Cu}(\text{OH})_2$ (aq) in the aqueous system. The lower solubility of $\text{Cu}(\text{OH})_2$ (aq) might have contributed to the higher copper adsorption. At pH 12, the major species in the water system was $\text{Cu}(\text{OH})_3^-$. The presence of negatively charged species may repel the negatively charged TP, which may have resulted in low copper removal (1.26%).

4.8 Effect on Heavy Metal Transport

Heavy metals move through several environmental compartments (air, water, soil, and biota). They pollute and accumulate, moving through different compartments. The change in the sinks and remobilization processes requires a further risk assessment.

Heavy metals tend to be less water soluble but have the ability to adsorb onto particulate matter or bind to organic groups. As a result, they can be found in sediments, animals, and plants. The majority of the dissolved heavy metals are adsorbed onto particulate matter due to the physicochemical properties of the metals. The clay and organic compounds in water can adsorb heavy metals. The positively charged metals interact with the negatively charged groups of clay (silicon hydroxides, aluminum hydroxides) and organic compounds (manganese oxides, carboxy, and phenolic groups) (Pachana et al., 2010). Heavy metal adsorbed onto bottom sediments may be released due to chemical changes in water (Förstner & Wittmann, 1981). Heavy metals could also be sorbed by mobile colloids in the solid phase. Stable colloids can facilitate heavy metal transport over a long distance. The huge generation of TP is making them ubiquitous in nature. TP are a new source of colloids in water. The results from this study indicated that heavy metals could adsorb on TP. Colloidal TP can facilitate transport for heavy metals.

However, more studies are needed to ascertain if TP could form stable colloids for heavy metal transport.

4.9 Insights into the Adsorption Mechanisms

Previous studies have investigated possible mechanisms involved in heavy metal adsorption on different adsorbents (S. Liu et al., 2022) (Shahrokhi-Shahraki et al., 2021) (J. Xu et al., 2018) . The possible mechanisms thought to be involved when heavy metals adsorb on typical adsorbents are a) physical adsorption, b) ion exchange, c) electrostatic attraction, and d) surface complexation. Zeta potential results in this study showed that electrostatic attraction was a possible mechanism for the adsorption of heavy metals on TP. pH, FT-IR and XPS results indicated that surface complexation was a possible mechanism. The adsorption isotherms for heavy metals were comparable for TP with two different BET surface areas. This indicated that the adsorption was not controlled by the physical process. For the ion-exchange process, adsorbents are usually porous and functionalized. The SEM images of the TP revealed that the particles were non-porous in nature. Ion exchange might not have been a primary mechanism as a result. In order to confirm that ion exchange was not a primary mechanism, more research is required.

Chapter 5: Conclusion and future work

5.1 Conclusion

In this study, the adsorption capacity of TP for heavy metals (lead and copper) was evaluated in single and competitive adsorption tests. pH effect on the adsorption of heavy metals on aged TP was examined. The possible adsorption mechanisms involved in the adsorption of heavy metals on TP were investigated through pH, zeta potential, FT-IR, and XPS results. The main conclusions from the study are as follows:

- 1) The untreated and aged TP in this study were nonporous and irregular in shape. The TP size ranged from 1 μm to many hundreds of micrometers. The BET surface area of the untreated and aged TP was 0.15 and 0.28 m^2/g , respectively.
- 2) The point of zero charge (pH_{pzc}) of the aged TP was pH 2. At the experimental pH (pH 6.2), the aged TP were negatively charged. Hence, electrostatic attraction was a possible mechanism for the adsorption of positively charged metal ions on negatively charged TP.
- 3) The zeta potential of the aged TP hardly changed after heavy metal adsorption compared to the initial value. Previous studies indicated that the adsorption of ions on the diffuse layer does not change the zeta potential and occurs by electrostatic attraction (Shahrokhi-Shahraki et al., 2021) (Wakatsuki et al., 1974). Electrostatic attraction was considered as a possible adsorption mechanism as a result.
- 4) FT-IR results indicated that there was a change in the peak for $-\text{N}=\text{C}=\text{O}$ (isocyanate) and $\text{C}=\text{O}$ (Carbonyl) groups in aged TP after heavy metal adsorption.

Previous studies suggested that oxygen-containing groups and/or aromatic π -electrons are involved in the surface complexation of heavy metals (Hotová et al., 2020). The FT-IR results indicated that surface complexation was a possible mechanism for the adsorption of heavy metals on aged TP.

- 5) XPS spectra of aged TP was analyzed before and after lead adsorption in this study. The copper-adsorbed aged TP was not examined since the adsorption was below the XPS instrument detection limit. After lead adsorption on aged TP, the relative content of the (O-C=O) group increased from 80.34 to 89.73% and the (C-O) group decreased from 19.66 to 10.27% for O 1s XPS spectra. The change was attributed to the formation of $\text{Pb}^{2+}\text{-O-C=O}$ or Pb-O functional groups on the surface of aged TP (Shahrokhi-Shahraki et al., 2021) (Guo et al., 2018). As a result, surface complexation was considered as a possible adsorption mechanism.
- 6) In single batch adsorption tests, the adsorption of the heavy metals on untreated and aged TP was comparable. The untreated and aged TP had different BET surface areas. This indicated that the adsorption was not controlled by the physical process.
- 7) In single batch adsorption tests, the Langmuir model was the better fit for the adsorption of lead on untreated TP. The maximum adsorption capacity (Q_m) was 11.054 mg/g. For the adsorption of lead on aged TP, the Freundlich model was the better fit. The adsorption capacity parameter (K_f) was $8.433 \text{ (mg/g)/(mg/L)}^{1/n}$. The Freundlich model was the better fit for both untreated and aged TP for copper

adsorption. For copper adsorption, the adsorption capacity parameter (K_f) for untreated and aged TP was 0.614 and 0.517 $(\text{mg/g})/(\text{mg/L})^{1/n}$, respectively.

- 8) In this study, aged TP was used in the competitive adsorption of the heavy metals. The Freundlich model was the better fit for both lead and copper. The adsorption capacity parameter (K_f) for lead and copper was 2.933 and 0.179 $(\text{mg/g})/(\text{mg/L})^{1/n}$, respectively for competitive adsorption.
- 9) Lead had a stronger affinity for TP than copper in both competitive and single adsorption. In comparison to a single metal system, the dual metal system exhibited a decrease in the adsorption capacity of TP for both metals.
- 10) The effect of pH on the adsorption was strong. Strong pH dependence shows that surface complexation plays a significant role in adsorption, according to previous investigations (Bradbury & Baeyens, 2002) (Um & Papeis, 2003) (D. Xu et al., 2008). Hence, surface complexation was a possible adsorption mechanism. The adsorption capacity of aged TP was maximum at the pH range of 6-12 for lead and at pH 10 for copper.
- 11) pH, zeta potential, FT-IR, and XPS results showed that electrostatic attraction and surface complexation were possible mechanisms in the adsorption of heavy metals on TP.
- 12) The studied TP had a higher adsorption capacity for heavy metals than microplastics but a lower adsorption capacity than conventional adsorbents. The TP used in this study cannot be used as a conventional adsorbent for heavy metals without treatment. Microplastics are argued to be vectors for heavy metals

(Brennecke et al., 2016) (Abbasi et al., 2020). Considering the ubiquitous nature of TP, they have the potential to be vectors of heavy metals in terms of adsorption capacity. However, it is unclear if TP can significantly alter the bioavailability and toxicity of heavy metals outcompeting more prevalent inorganic/organic particulate matter.

5.2 Future work

This project should logically lead to, but not be limited to, the following investigations:

- 1) This study focused on the adsorption capacity of TP to investigate the vector effect of TP for heavy metals. Further studies are required to investigate the extent to which TP can affect the bioavailability and toxicity of heavy metals.
- 2) pH effect on the adsorption of heavy metal on TP was investigated in this study. The effects of the nature of the adsorbent (particle size, different aging process, adsorbent dose) and environmental factors (ionic strength, organic matter, the presence of other contaminants, and salinity) on the adsorption process need to be investigated.
- 3) The TP used in this study were cryo-milled. There is a difference in shape and density of cryo-milled with environmental TP. The environmental TP go through heteroaggregation combining with minerals and dust derived from the road surface. The adsorption properties of the environmental TP need to be investigated.

- 4) Tire materials are reported to leach zinc (Rhodes et al., 2012) (Degaffe & Turner, 2011) and toxic polycyclic aromatic hydrocarbons (PAHs) (Wachtendorf et al., 2017) to the environment. More research is required to investigate the potential leaching of chemicals from TP.
- 5) This study investigated the adsorption of lead and copper on TP in the single and dual metal system. Further studies are required to evaluate the adsorption behavior of other toxic metals on TP.
- 6) Electrostatic attraction and surface complexation were identified as possible adsorption mechanisms in this study. Further tests are required to confirm the involvement of physical adsorption/ion exchange in the adsorption process.
- 7) Langmuir and Freundlich models were used to describe the adsorption data in the study. Other models can be evaluated which might better describe the adsorption process.
- 8) Bicarbonates, Cl^- , SO_4^{2-} , and complexes of metals/natural organics are examples of common ions and complexes that are present in natural water. The impact of these chemical species on the adsorption process needs to be investigated.

References

- Abbasi, S., Moore, F., Keshavarzi, B., Hopke, P. K., Naidu, R., Rahman, M. M., Oleszczuk, P., & Karimi, J. (2020). PET-microplastics as a vector for heavy metals in a simulated plant rhizosphere zone. *Science of The Total Environment*, 744, 140984. <https://doi.org/10.1016/j.scitotenv.2020.140984>
- Abdolahpur Monikh, F., Vijver, M. G., Guo, Z., Zhang, P., Darbha, G. K., & Peijnenburg, W. J. G. M. (2020). Metal sorption onto nanoscale plastic debris and trojan horse effects in *Daphnia magna*: Role of dissolved organic matter. *Water Research*, 186, 116410. <https://doi.org/10.1016/j.watres.2020.116410>
- Aboelkheir, M. G., Bedor, P. B., Leite, S. G., Pal, K., Toledo Filho, R. D., & Gomes de Souza, F. (2019). Biodegradation of Vulcanized SBR: A Comparison between *Bacillus subtilis*, *Pseudomonas aeruginosa* and *Streptomyces* sp. *Scientific Reports*, 9(1), 19304. <https://doi.org/10.1038/s41598-019-55530-y>
- Abollino, O., Aceto, M., Malandrino, M., Sarzanini, C., & Mentasti, E. (2003). Adsorption of heavy metals on Na-montmorillonite. Effect of pH and organic substances. *Water Research*, 37(7), 1619–1627. [https://doi.org/10.1016/S0043-1354\(02\)00524-9](https://doi.org/10.1016/S0043-1354(02)00524-9)
- Alamo-Nole, L., Perales-Perez, O., & Roman, F. R. (2012). Use of recycled tires crumb rubber to remove organic contaminants from aqueous and gaseous phases. *Desalination and Water Treatment*, 49(1–3), 296–306. <https://doi.org/10.1080/19443994.2012.719350>

- Al-Asheh, S., & Banat, F. (2000). Adsorption of Copper Ions on to Tyre Rubber. *Adsorption Science & Technology*, 18(8), 685–700.
<https://doi.org/10.1260/0263617001493738>
- Ali, U. F. M., Hussin, F., Gopinath, S. C. B., Aroua, M. K., Khamidun, M. H., Jusoh, N., Ibrahim, N., & Ahmad, S. F. K. (2021). Advancement in recycling waste tire activated carbon to potential adsorbents. *Environmental Engineering Research*, 27(6), 210452–0. <https://doi.org/10.4491/eer.2021.452>
- Ashton, K., Holmes, L., & Turner, A. (2010). Association of metals with plastic production pellets in the marine environment. *Marine Pollution Bulletin*, 60(11), 2050–2055. <https://doi.org/10.1016/j.marpolbul.2010.07.014>
- Bradbury, M. H., & Baeyens, B. (2002). Sorption of Eu on Na- and Ca-montmorillonites: Experimental investigations and modelling with cation exchange and surface complexation. *Geochimica et Cosmochimica Acta*, 66(13), 2325–2334.
[https://doi.org/10.1016/S0016-7037\(02\)00841-4](https://doi.org/10.1016/S0016-7037(02)00841-4)
- Cadle, S., & Williams, R. (1980). Environmental degradation of tire-wear particles. *Rubber Chemistry and Technology*, 53(4), 903–914.
- Cao, Y., Zhao, M., Ma, X., Song, Y., Zuo, S., Li, H., & Deng, W. (2021). A critical review on the interactions of microplastics with heavy metals: Mechanism and their combined effect on organisms and humans. *Science of The Total Environment*, 788, 147620. <https://doi.org/10.1016/j.scitotenv.2021.147620>

- Chen, Wright, J. V., Conca, J. L., & Peurrung, L. M. (1997). Effects of pH on Heavy Metal Sorption on Mineral Apatite. *Environmental Science & Technology*, 31(3), 624–631. <https://doi.org/10.1021/es950882f>
- Chen, X., Hossain, M. F., Duan, C., Lu, J., Tsang, Y. F., Islam, M. S., & Zhou, Y. (2022). Isotherm models for adsorption of heavy metals from water—A review. *Chemosphere*, 307, 135545. <https://doi.org/10.1016/j.chemosphere.2022.135545>
- Cho, H.-H., Smith, B. A., Wnuk, J. D., Fairbrother, D. H., & Ball, W. P. (2008). Influence of Surface Oxides on the Adsorption of Naphthalene onto Multiwalled Carbon Nanotubes. *Environmental Science & Technology*, 42(8), 2899–2905. <https://doi.org/10.1021/es702363e>
- Cocchi, M., Foca, G., Lucisano, M., Marchetti, A., Pagani, M. A., Tassi, L., & Ulrici, A. (2004). Classification of cereal flours by chemometric analysis of MIR spectra. *Journal of Agricultural and Food Chemistry*, 52(5), 1062–1067.
- European Commission. Joint Research Centre. Institute for Energy and Transport. (2014). *Non-exhaust traffic related emissions - Brake and tyre wear PM: Literature review*. Publications Office. <https://data.europa.eu/doi/10.2790/21481>
- Fan, X., Ma, Z., Zou, Y., Liu, J., & Hou, J. (2021). Investigation on the adsorption and desorption behaviors of heavy metals by tire wear particles with or without UV ageing processes. *Environmental Research*, 195, 110858. <https://doi.org/10.1016/j.envres.2021.110858>
- Förstner, U., & Wittmann, G. T. W. (1981). *Metal Pollution in the Aquatic Environment*. Springer Berlin Heidelberg. <https://doi.org/10.1007/978-3-642-69385-4>

- Fu, Q., Tan, X., Ye, S., Ma, L., Gu, Y., Zhang, P., Chen, Q., Yang, Y., & Tang, Y. (2021). Mechanism analysis of heavy metal lead captured by natural-aged microplastics. *Chemosphere*, 270, 128624. <https://doi.org/10.1016/j.chemosphere.2020.128624>
- Godoy, V., Blázquez, G., Calero, M., Quesada, L., & Martín-Lara, M. A. (2019). The potential of microplastics as carriers of metals. *Environmental Pollution*, 255, 113363. <https://doi.org/10.1016/j.envpol.2019.113363>
- Goel, J., Kadirvelu, K., Rajagopal, C., & Kumar Garg, V. (2005). Removal of lead(II) by adsorption using treated granular activated carbon: Batch and column studies. *Journal of Hazardous Materials*, 125(1–3), 211–220. <https://doi.org/10.1016/j.jhazmat.2005.05.032>
- Guo, S., Dan, Z., Duan, N., Chen, G., Gao, W., & Zhao, W. (2018). Zn(II), Pb(II), and Cd(II) adsorption from aqueous solution by magnetic silica gel: Preparation, characterization, and adsorption. *Environmental Science and Pollution Research*, 25(31), 30938–30948. <https://doi.org/10.1007/s11356-018-3050-7>
- Halle, L. L., Palmqvist, A., Kampmann, K., Jensen, A., Hansen, T., & Khan, F. R. (2021). Tire wear particle and leachate exposures from a pristine and road-worn tire to *Hyalella azteca*: Comparison of chemical content and biological effects. *Aquatic Toxicology*, 232, 105769. <https://doi.org/10.1016/j.aquatox.2021.105769>
- Holmes, L. A., Turner, A., & Thompson, R. C. (2012). Adsorption of trace metals to plastic resin pellets in the marine environment. *Environmental Pollution*, 160, 42–48. <https://doi.org/10.1016/j.envpol.2011.08.052>

- Hotová, G., Slovák, V., Zelenka, T., Maršálek, R., & Parchaňská, A. (2020). The role of the oxygen functional groups in adsorption of copper (II) on carbon surface. *Science of The Total Environment*, 711, 135436. <https://doi.org/10.1016/j.scitotenv.2019.135436>
- HUCZYNSKI, A., RATAJCZAK-SITARZ, M., STEFANSKA, J., KATRUSIAK, A., BRZEZINSKI, B., & BARTL, F. (2011). Infrared and Raman Characteristic Group Frequencies: Tables and Charts Infrared and Raman Characteristic Group Frequencies: Tables and Charts 154, 2004. *Journal of Antibiotics*, 64(3), 249–256.
- Hüffer, T., Praetorius, A., Wagner, S., von der Kammer, F., & Hofmann, T. (2017). Microplastic Exposure Assessment in Aquatic Environments: Learning from Similarities and Differences to Engineered Nanoparticles. *Environmental Science & Technology*, 51(5), 2499–2507. <https://doi.org/10.1021/acs.est.6b04054>
- Hüffer, T., Wagner, S., Reemtsma, T., & Hofmann, T. (2019). Sorption of organic substances to tire wear materials: Similarities and differences with other types of microplastic. *TrAC Trends in Analytical Chemistry*, 113, 392–401. <https://doi.org/10.1016/j.trac.2018.11.029>
- Kim, G., & Lee, S. (2018). Characteristics of Tire Wear Particles Generated by a Tire Simulator under Various Driving Conditions. *Environmental Science & Technology*, 52(21), 12153–12161. <https://doi.org/10.1021/acs.est.8b03459>
- Klößner, P., Seiwert, B., Wagner, S., & Reemtsma, T. (2021). Organic Markers of Tire and Road Wear Particles in Sediments and Soils: Transformation Products of

- Major Antiozonants as Promising Candidates. *Environmental Science & Technology*, 55(17), 11723–11732. <https://doi.org/10.1021/acs.est.1c02723>
- Klöckner, P., Seiwert, B., Weyrauch, S., Escher, B. I., Reemtsma, T., & Wagner, S. (2021). Comprehensive characterization of tire and road wear particles in highway tunnel road dust by use of size and density fractionation. *Chemosphere*, 279, 130530. <https://doi.org/10.1016/j.chemosphere.2021.130530>
- Koelmans, A. A., Bakir, A., Burton, G. A., & Janssen, C. R. (2016). Microplastic as a Vector for Chemicals in the Aquatic Environment: Critical Review and Model-Supported Reinterpretation of Empirical Studies. *Environmental Science & Technology*, 50(7), 3315–3326. <https://doi.org/10.1021/acs.est.5b06069>
- Kole, P. J., Löhr, A. J., Van Belleghem, F., & Ragas, A. (2017). Wear and Tear of Tyres: A Stealthy Source of Microplastics in the Environment. *International Journal of Environmental Research and Public Health*, 14(10), 1265. <https://doi.org/10.3390/ijerph14101265>
- Kolomijeca, A., Parrott, J., Khan, H., Shires, K., Clarence, S., Sullivan, C., Chibwe, L., Sinton, D., & Rochman, C. M. (2020). Increased Temperature and Turbulence Alter the Effects of Leachates from Tire Particles on Fathead Minnow (*Pimephales promelas*). *Environmental Science & Technology*, 54(3), 1750–1759. <https://doi.org/10.1021/acs.est.9b05994>
- Kreider, M. L., Panko, J. M., McAtee, B. L., Sweet, L. I., & Finley, B. L. (2010). Physical and chemical characterization of tire-related particles: Comparison of

- particles generated using different methodologies. *Science of The Total Environment*, 408(3), 652–659. <https://doi.org/10.1016/j.scitotenv.2009.10.016>
- Lee, S., Kwak, J., Kim, H., & Lee, J. (2013). Properties of roadway particles from interaction between the tire and road pavement. *International Journal of Automotive Technology*, 14(1), 163–173. <https://doi.org/10.1007/s12239-013-0018-y>
- Liang, S. B., & Hao, Y. C. (2000). A novel cryogenic grinding system for recycling scrap tire peels. *Advanced Powder Technology*, 11(2), 187–197. <https://doi.org/10.1163/156855200750172303>
- Liu, G., Dave, P. H., Kwong, R. W. M., Wu, M., & Zhong, H. (2021). Influence of Microplastics on the Mobility, Bioavailability, and Toxicity of Heavy Metals: A Review. *Bulletin of Environmental Contamination and Toxicology*, 107(4), 710–721. <https://doi.org/10.1007/s00128-021-03339-9>
- Liu, S., Huang, J., Zhang, W., Shi, L., Yi, K., Yu, H., Zhang, C., Li, S., & Li, J. (2022). Microplastics as a vehicle of heavy metals in aquatic environments: A review of adsorption factors, mechanisms, and biological effects. *Journal of Environmental Management*, 302, 113995. <https://doi.org/10.1016/j.jenvman.2021.113995>
- Luo, Z., Zhou, X., Su, Y., Wang, H., Yu, R., Zhou, S., Xu, E. G., & Xing, B. (2021). Environmental occurrence, fate, impact, and potential solution of tire microplastics: Similarities and differences with tire wear particles. *Science of The Total Environment*, 795, 148902. <https://doi.org/10.1016/j.scitotenv.2021.148902>

- Mao, R., Lang, M., Yu, X., Wu, R., Yang, X., & Guo, X. (2020). Aging mechanism of microplastics with UV irradiation and its effects on the adsorption of heavy metals. *Journal of Hazardous Materials*, *393*, 122515. <https://doi.org/10.1016/j.jhazmat.2020.122515>
- McCarthy, J. F., & Zachara, J. M. (1989). Subsurface transport of contaminants. *Environmental Science & Technology*, *23*(5), 496–502. <https://doi.org/10.1021/es00063a001>
- McPherson, A. T., & Cummings, A. D. (1935). Refractive index of rubber. *Rubber Chemistry and Technology*, *8*(3), 421–429.
- Mosca Angelucci, D., & Tomei, M. C. (2022). Uptake/release of organic contaminants by microplastics: A critical review of influencing factors, mechanistic modeling, and thermodynamic prediction methods. *Critical Reviews in Environmental Science and Technology*, *52*(8), 1356–1400. <https://doi.org/10.1080/10643389.2020.1856594>
- Mousavi, H. Z., Hosseynifar, A., Jahed, V., & Dehghani, S. A. M. (2010). Removal of lead from aqueous solution using waste tire rubber ash as an adsorbent. *Brazilian Journal of Chemical Engineering*, *27*(1), 79–87. <https://doi.org/10.1590/S0104-66322010000100007>
- Müller, K., Hübner, D., Huppertsberg, S., Knepper, T. P., & Zahn, D. (2022). Probing the chemical complexity of tires: Identification of potential tire-borne water contaminants with high-resolution mass spectrometry. *Science of The Total Environment*, *802*, 149799. <https://doi.org/10.1016/j.scitotenv.2021.149799>

- Pachana, K., Wattanakornsiri, A., & Nanuam, J. (2010). Heavy metal transport and fate in the environmental compartments. *NU. International Journal of Science*, 7(1), 1–11.
- Park, J.-H., Ok, Y. S., Kim, S.-H., Cho, J.-S., Heo, J.-S., Delaune, R. D., & Seo, D.-C. (2016). Competitive adsorption of heavy metals onto sesame straw biochar in aqueous solutions. *Chemosphere*, 142, 77–83.
<https://doi.org/10.1016/j.chemosphere.2015.05.093>
- Pehlken, A., & Elhachmi Essadiqi. (2005). *Scrap Tire Recycling in Canada*.
<https://doi.org/10.13140/2.1.1941.8400>
- Powell, K. J., Brown, P. L., Byrne, R. H., Gajda, T., Hefter, G., Leuz, A.-K., Sjöberg, S., & Wanner, H. (2009). Chemical speciation of environmentally significant metals with inorganic ligands. Part 3: The $Pb^{2++} OH^-$, Cl^- , CO_3^{2-} , SO_4^{2-} , and PO_4^{3-} systems (IUPAC Technical Report). *Pure and Applied Chemistry*, 81(12), 2425–2476.
- Powell, K. J., Brown, P. L., Byrne, R. H., Gajda, T., Hefter, G., Sjöberg, S., & Wanner, H. (2007). Chemical speciation of environmentally significant metals with inorganic ligands Part 2: The $Cu^{2+-}OH^-$, Cl^- , CO_3^{2-} , SO_4^{2-} , and PO_4^{3-} systems (IUPAC Technical Report). *Pure and Applied Chemistry*, 79(5), 895–950.
- Rajiv Gandhi, M., & Meenakshi, S. (2012). Preparation and characterization of silica gel/chitosan composite for the removal of Cu(II) and Pb(II). *International Journal of Biological Macromolecules*, 50(3), 650–657.
<https://doi.org/10.1016/j.ijbiomac.2012.01.012>

- Rodda, D. P., Johnson, B. B., & Wells, J. D. (1993). The effect of temperature and pH on the adsorption of copper (II), lead (II), and zinc (II) onto goethite. *Journal of Colloid and Interface Science*, *161*(1), 57–62.
- Rosca, I. D., Watari, F., Uo, M., & Akasaka, T. (2005). Oxidation of multiwalled carbon nanotubes by nitric acid. *Carbon*, *43*(15), 3124–3131.
<https://doi.org/10.1016/j.carbon.2005.06.019>
- Sadiktsis, I., Bergvall, C., Johansson, C., & Westerholm, R. (2012). Automobile Tires—A Potential Source of Highly Carcinogenic Dibenzopyrenes to the Environment. *Environmental Science & Technology*, *46*(6), 3326–3334.
<https://doi.org/10.1021/es204257d>
- Shahrokhi-Shahraki, R., Benally, C., El-Din, M. G., & Park, J. (2021). High efficiency removal of heavy metals using tire-derived activated carbon vs commercial activated carbon: Insights into the adsorption mechanisms. *Chemosphere*, *264*, 128455. <https://doi.org/10.1016/j.chemosphere.2020.128455>
- Sivaraman, S., Michael Anbuselvan, N., Venkatachalam, P., Ramiah Shanmugam, S., & Selvasembian, R. (2022). Waste tire particles as efficient materials towards hexavalent chromium removal: Characterisation, adsorption behaviour, equilibrium, and kinetic modelling. *Chemosphere*, *295*, 133797.
<https://doi.org/10.1016/j.chemosphere.2022.133797>
- Smith, B. (2022). Infrared Spectroscopy of Polymers, VIII: Polyesters and the Rule of Three. *Spectroscopy*, *37*(10), 25–28.

- Sommer, F., Dietze, V., Baum, A., Sauer, J., Gilge, S., Maschowski, C., & Gieré, R. (2018). Tire Abrasion as a Major Source of Microplastics in the Environment. *Aerosol and Air Quality Research*, 18(8), 2014–2028. <https://doi.org/10.4209/aaqr.2018.03.0099>
- Tang, S., Lin, L., Wang, X., Yu, A., & Sun, X. (2021). Interfacial interactions between collected nylon microplastics and three divalent metal ions (Cu (II), Ni (II), Zn (II)) in aqueous solutions. *Journal of Hazardous Materials*, 403, 123548.
- Turner, A., & Holmes, L. A. (2015). Adsorption of trace metals by microplastic pellets in fresh water. *Environmental Chemistry*, 12(5), 600–610.
- Um, W., & Papeis, C. (2003). Sorption mechanisms of Sr and Pb on zeolitized tuffs from the Nevada test site as a function of pH and ionic strength. *American Mineralogist*, 88(11–12), 2028–2039.
- Unice, K. M., Bare, J. L., Kreider, M. L., & Panko, J. M. (2015). Experimental methodology for assessing the environmental fate of organic chemicals in polymer matrices using column leaching studies and OECD 308 water/sediment systems: Application to tire and road wear particles. *Science of The Total Environment*, 533, 476–487. <https://doi.org/10.1016/j.scitotenv.2015.06.053>
- Wachtendorf, V., Kalbe, U., Krüger, O., & Bandow, N. (2017). Influence of weathering on the leaching behaviour of zinc and PAH from synthetic sports surfaces. *Polymer Testing*, 63, 621–631. <https://doi.org/10.1016/j.polymertesting.2017.09.021>

- Wagner, S., Hüffer, T., Klöckner, P., Wehrhahn, M., Hofmann, T., & Reemtsma, T. (2018). Tire wear particles in the aquatic environment—A review on generation, analysis, occurrence, fate and effects. *Water Research*, *139*, 83–100. <https://doi.org/10.1016/j.watres.2018.03.051>
- Wagner, S., Klöckner, P., & Reemtsma, T. (2022). Aging of tire and road wear particles in terrestrial and freshwater environments – A review on processes, testing, analysis and impact. *Chemosphere*, *288*, 132467. <https://doi.org/10.1016/j.chemosphere.2021.132467>
- Wakatsuki, T., Furukawa, H., & Kawaguchi, K. (1974). Specific and non-specific adsorption of inorganic ions I. Evaluation of specific adsorbability by means of minimum concentration for specific adsorption. *Soil Science and Plant Nutrition*, *20*(4), 353–362. <https://doi.org/10.1080/00380768.1974.10432606>
- Wang, Q., Zhang, Y., Wangjin, X., Wang, Y., Meng, G., & Chen, Y. (2020). The adsorption behavior of metals in aqueous solution by microplastics effected by UV radiation. *Journal of Environmental Sciences*, *87*, 272–280. <https://doi.org/10.1016/j.jes.2019.07.006>
- What's In a Tire* | U.S. Tire Manufacturers Association. (n.d.). Retrieved January 6, 2023, from <https://www.ustires.org/whats-tire-0>
- Wu, J., Wang, T., Zhang, Y., & Pan, W.-P. (2019). The distribution of Pb(II)/Cd(II) adsorption mechanisms on biochars from aqueous solution: Considering the increased oxygen functional groups by HCl treatment. *Bioresource Technology*, *291*, 121859. <https://doi.org/10.1016/j.biortech.2019.121859>

- Xu, D., Tan, X. L., Chen, C. L., & Wang, X. K. (2008). Adsorption of Pb(II) from aqueous solution to MX-80 bentonite: Effect of pH, ionic strength, foreign ions and temperature. *Applied Clay Science*, *41*(1), 37–46.
<https://doi.org/10.1016/j.clay.2007.09.004>
- Xu, J., Cao, Z., Zhang, Y., Yuan, Z., Lou, Z., Xu, X., & Wang, X. (2018). A review of functionalized carbon nanotubes and graphene for heavy metal adsorption from water: Preparation, application, and mechanism. *Chemosphere*, *195*, 351–364.
<https://doi.org/10.1016/j.chemosphere.2017.12.061>
- Xu, R., Xiao, S., Yuan, J., & Zhao, A. (2011). Adsorption of methyl violet from aqueous solutions by the biochars derived from crop residues. *Bioresource Technology*, *102*(22), 10293–10298. <https://doi.org/10.1016/j.biortech.2011.08.089>
- Zou, W., Han, R., Chen, Z., Shi, J., & Liu. (2006). Characterization and Properties of Manganese Oxide Coated Zeolite as Adsorbent for Removal of Copper(II) and Lead(II) Ions from Solution. *Journal of Chemical & Engineering Data*, *51*(2), 534–541. <https://doi.org/10.1021/jc0504008>

Appendix A: BET Surface Area Measurement Curves.

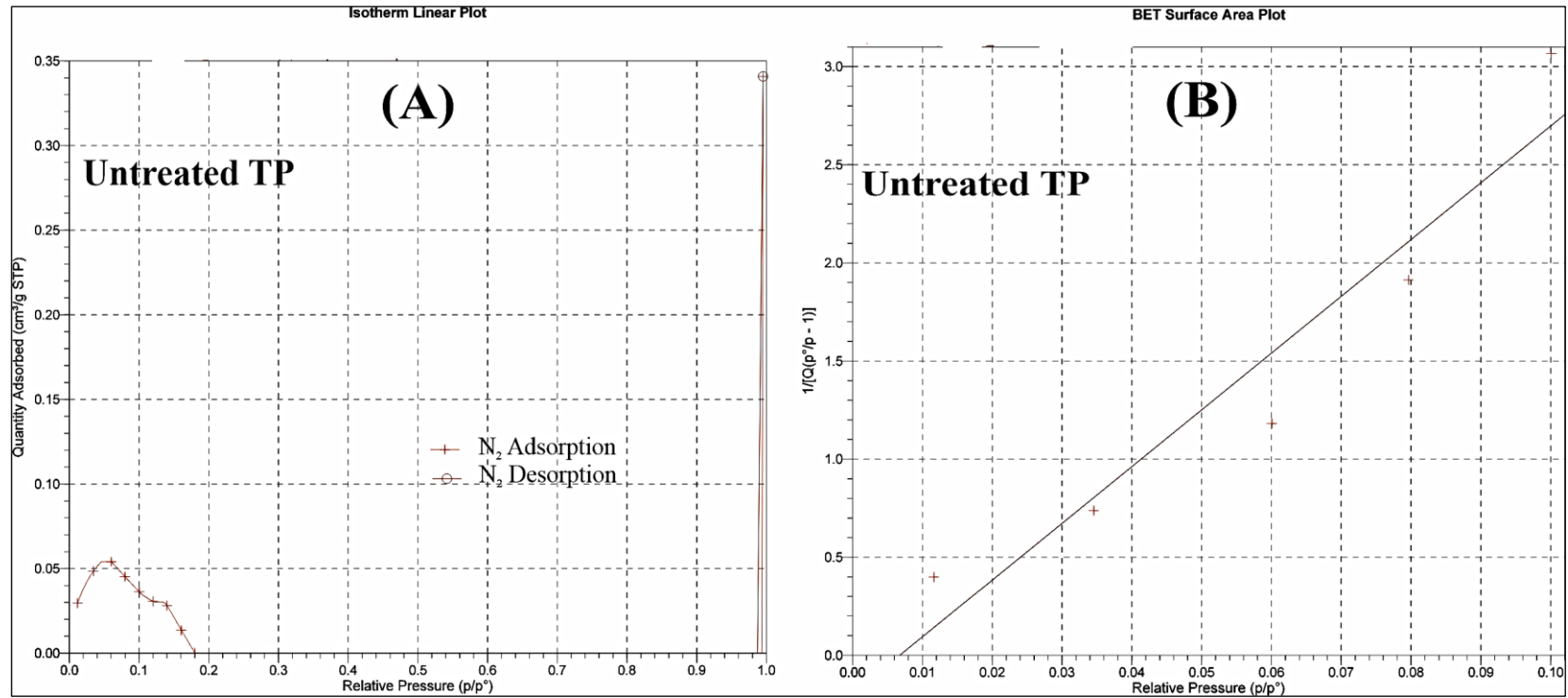


Figure 24.(A) N₂ adsorption-desorption isotherm and (B) correlation coefficient curve in measurement of BET surface area of untreated TP.

Summary Report	
Surface Area	
Single point surface area at $p/p^\circ = 0.100086502$:	0.1421 m ² /g
BET Surface Area:	0.1515 m ² /g
t-Plot Micropore Area:	1.0504 m ² /g
t-Plot External Surface Area:	-0.8989 m ² /g
Pore Volume	
Single point adsorption total pore volume of pores less than 4120.876 Å width at $p/p^\circ = 0.995303504$:	0.000527 cm ³ /g
t-Plot micropore volume:	0.000389 cm ³ /g
Pore Size	
Adsorption average pore width (4V/A by BET):	139.2121 Å

Figure 25. Summary report from Surface BET measurement for untreated TP.

BET Surface Area Report		
BET Surface Area: 0.1515 ± 0.0265 m ² /g		
Slope: 28.933086 ± 5.021297 g/cm ³ STP		
Y-Intercept: -0.195674 ± 0.327728 g/cm ³ STP		
C: -146.863929		
Qm: 0.0348 cm ³ /g STP		
Correlation Coefficient: 0.9576693		
Molecular Cross-Sectional Area: 0.1620 nm ²		
Relative Pressure (p/p [°])	Quantity Adsorbed (cm ³ /g STP)	1/[Q(p [°] /p - 1)]
0.011654401	0.0295	0.399384
0.034544551	0.0485	0.737623
0.060065540	0.0541	1.180969
0.079654962	0.0452	1.912815
0.100086502	0.0363	3.065876

Figure 26. BET surface area report from Surface BET measurement for untreated TP.

t-Plot Report

Micropore Volume: 0.000389 cm³/g
 Micropore Area: 1.0504 m²/g
 External Surface Area: -0.8989 m²/g
 Slope: -0.058116 ± 0.007707 cm³/g·Å STP
 Y-Intercept: 0.251725 ± 0.030041 cm³/g STP
 Correlation Coefficient: -0.966578
 Surface Area Correction Factor: 1.000
 Density Conversion Factor: 0.0015468
 Total Surface Area (BET): 0.1515 m²/g
 Thickness Range: 3.5000 Å to 5.0000 Å
 Thickness Equation: Harkins and Jura
 $t = [13.99 / (0.034 - \log(p/p^0))] ^ 0.5$

Relative Pressure (p/p ⁰)	Statistical Thickness (Å)	Quantity Adsorbed (cm ³ /g STP)	Fitted
0.011654401	2.6666	0.0295	
0.034544551	3.0584	0.0485	
0.060065540	3.3383	0.0541	
0.079654962	3.5143	0.0452	*
0.100086502	3.6790	0.0363	*
0.120085855	3.8284	0.0306	*
0.139998066	3.9695	0.0281	*
0.160584102	4.1098	0.0136	*
0.180049108	4.2389	0.0002	*

Figure 27. t-plot report from BET surface area measurement for untreated TP.

Summary Report

Surface Area

Single point surface area at p/p⁰ = 0.100133805: 0.2476 m²/g
 BET Surface Area: 0.2759 m²/g
 t-Plot Micropore Area: 0.6460 m²/g
 t-Plot External Surface Area: -0.3701 m²/g

BJH Adsorption cumulative surface area of pores between 17.000 Å and 3000.000 Å width: 0.102 m²/g

Pore Volume

Single point adsorption total pore volume of pores less than 4189.705 Å width at p/p⁰ = 0.995381375: 0.003208 cm³/g
 t-Plot micropore volume: 0.000239 cm³/g
 BJH Adsorption cumulative volume of pores between 17.000 Å and 3000.000 Å width: 0.003152 cm³/g

Pore Size

Adsorption average pore width (4V/A by BET): 465.0260 Å
 BJH Adsorption average pore width (4V/A): 1241.020 Å

Figure 28. Summary report from surface BET measurement of Aged TP.

BET Surface Area Report

BET Surface Area: 0.2759 ± 0.0166 m²/g
Slope: 15.656946 ± 0.946318 g/cm³ STP
Y-Intercept: 0.120969 ± 0.063559 g/cm³ STP
C: 130.429715
Qm: 0.0634 cm³/g STP
Correlation Coefficient: 0.9945650
Molecular Cross-Sectional Area: 0.1620 nm²

Relative Pressure (p/p°)	Quantity Adsorbed (cm ³ /g STP)	1/[Q(p°/p - 1)]
0.011695873	0.0355	0.333043
0.034887148	0.0535	0.675436
0.069042553	0.0663	1.119391
0.080048329	0.0646	1.347848
0.100133805	0.0632	1.760570

Figure 29. BET Surface area report from BET measurement of aged TP.

BJH Adsorption Pore Distribution Report

Faas Correction
Halsey
 $t = 3.54 [-5 / \ln(p/p^{\circ})] ^{0.333}$
Width Range: 17.000 Å to 3000.000 Å
Adsorbate Property Factor: 9.53000 Å
Density Conversion Factor: 0.0015468
Fraction of Pores Open at Both Ends: 0.00

Pore Width Range (Å)	Average Width (Å)	Incremental Pore Volume (cm ³ /g)	Cumulative Pore Volume (cm ³ /g)	Incremental Pore Area (m ² /g)	Cumulative Pore Area (m ² /g)
4157.2 - 2323.1	2758.6	0.002460	0.002460	0.036	0.036
2323.1 - 1062.1	1280.3	0.000673	0.003132	0.021	0.057
1062.1 - 17.5	17.9	0.000020	0.003152	0.045	0.102

Figure 30. Pore distribution report from BET surface area measurements of aged TP.

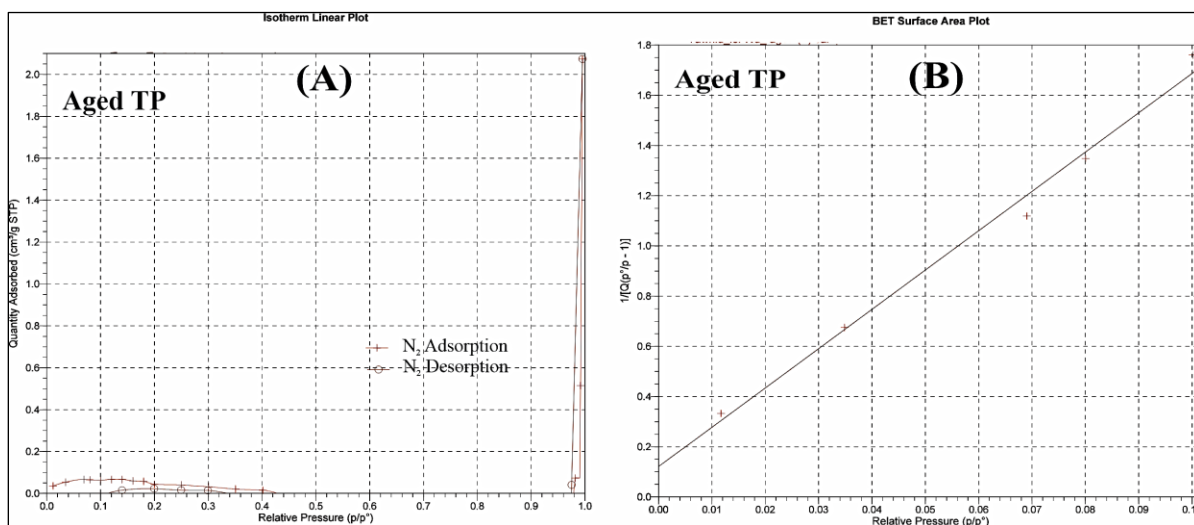


Figure 31. N₂ adsorption-desorption isotherm and (B) correlation coefficient curve in measurement of BET surface area of aged TP.

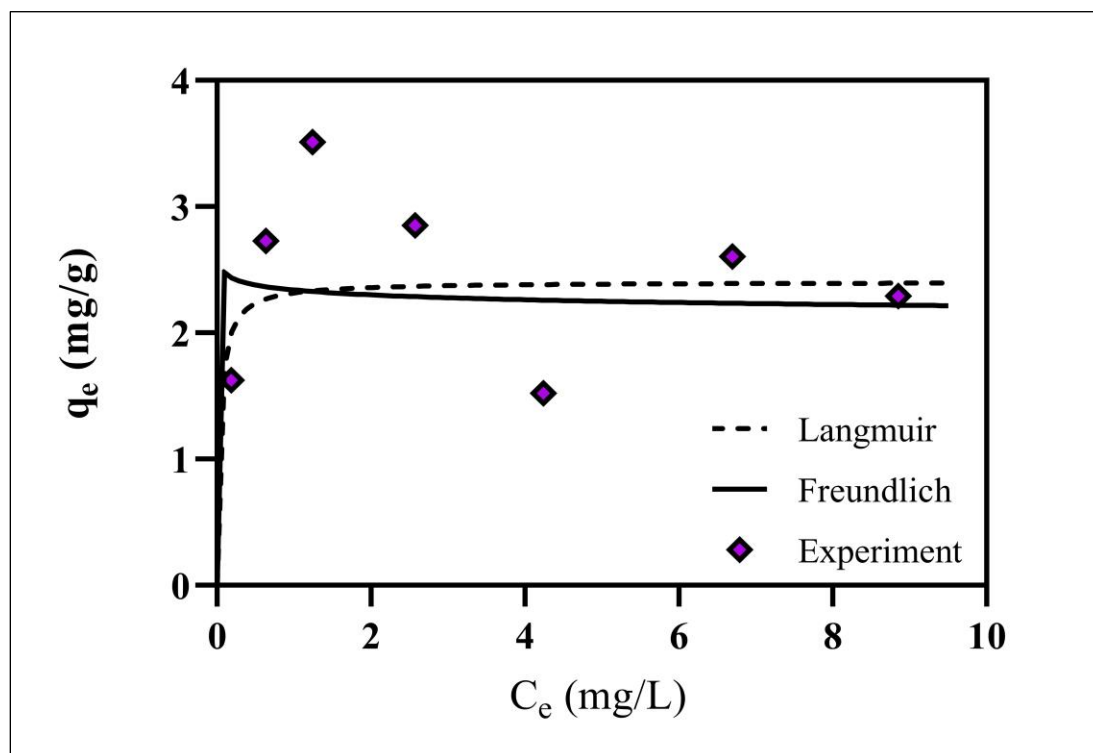
Appendix B: Screening Test for Adsorbent Dose Used in Isotherm Tests.

Figure 32. Adsorption data and fitted isotherm models for copper with 25 mg aged TP in 50 mL solution.

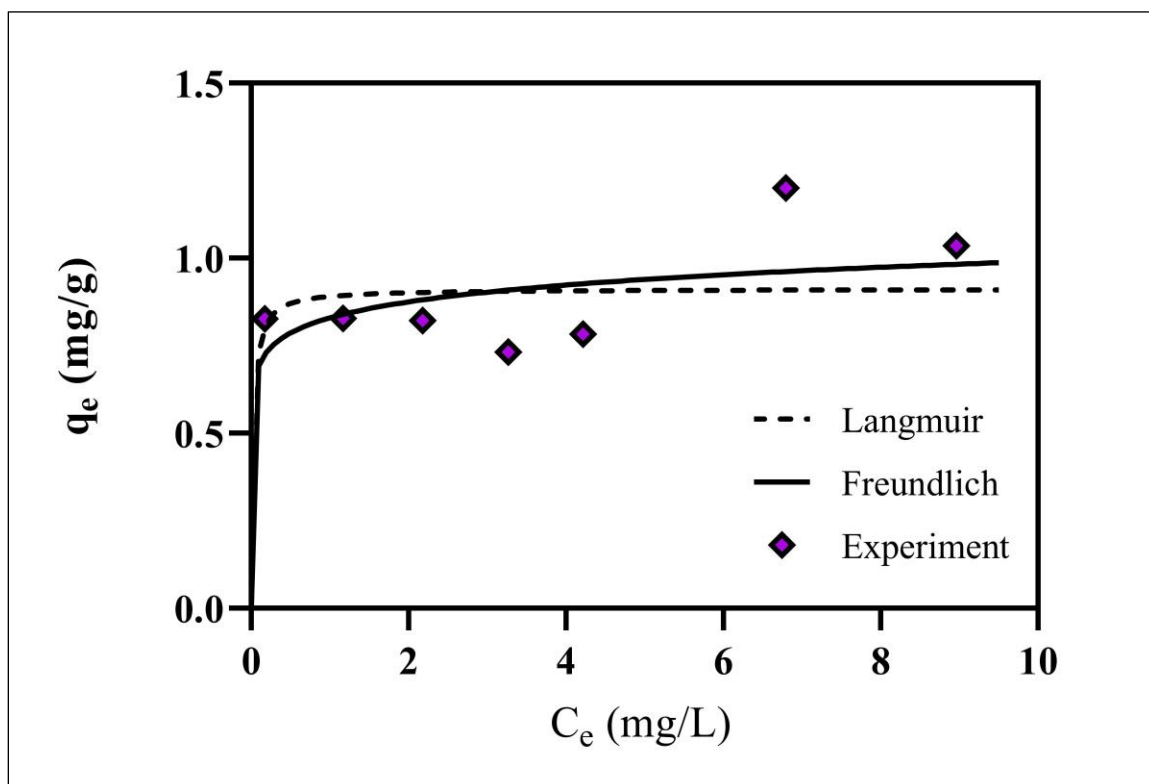


Figure 33. Adsorption data and fitted isotherm models for copper with 50 mg aged TP in 50 mL solution.

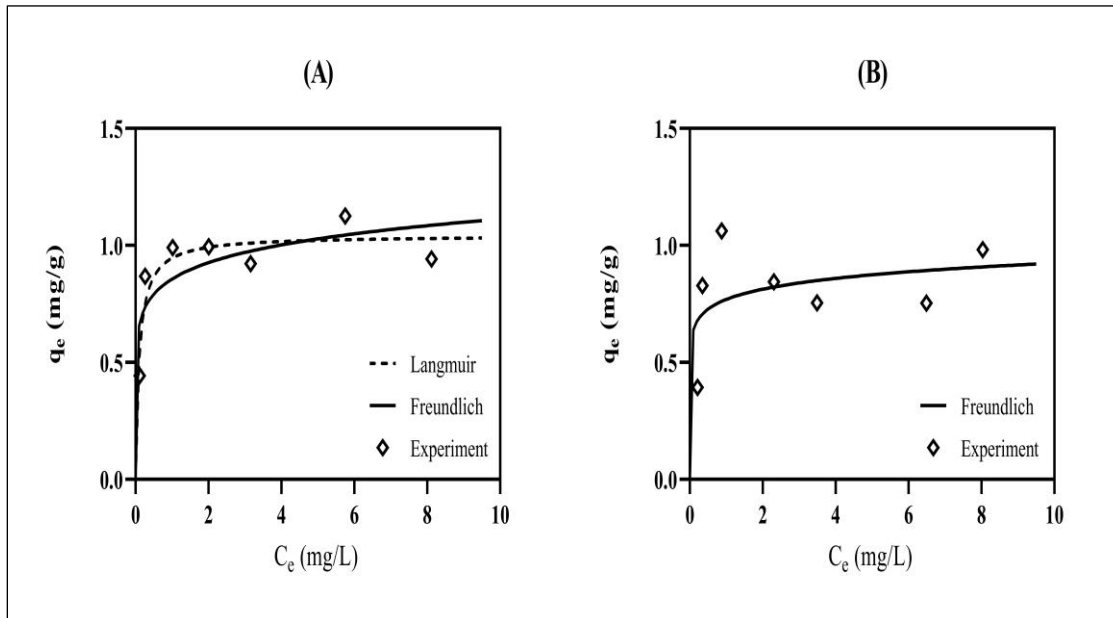


Figure 34.(A-B) Adsorption data and fitted isotherm models for copper with 100 mg untreated TP in 50 mL solution.

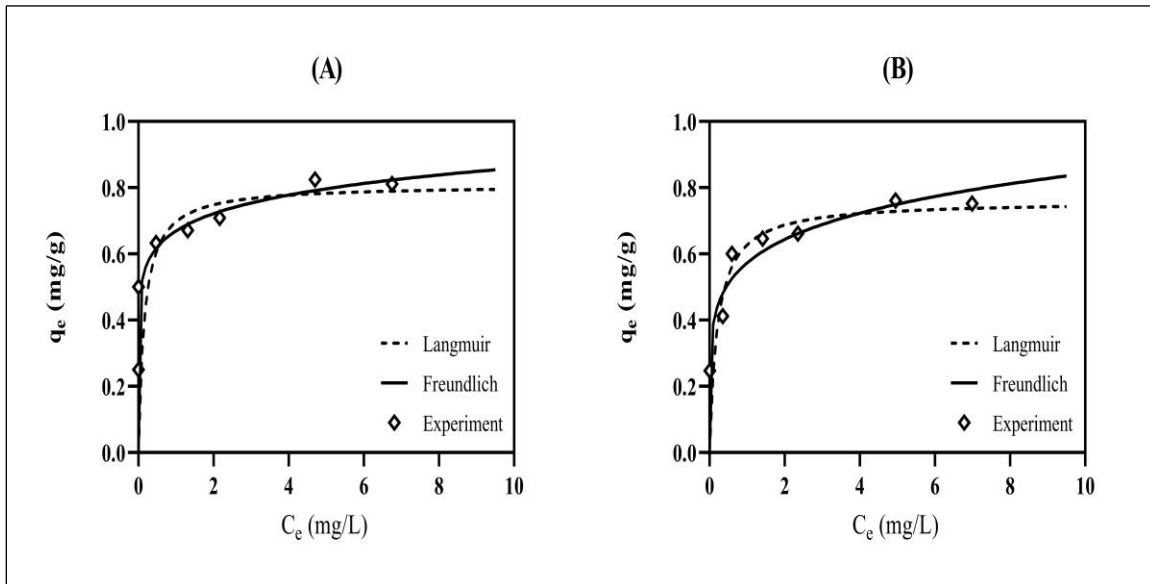


Figure 35(A-B) Adsorption data and fitted isotherm models for copper with 200 mg untreated TP in 50 mL solution.

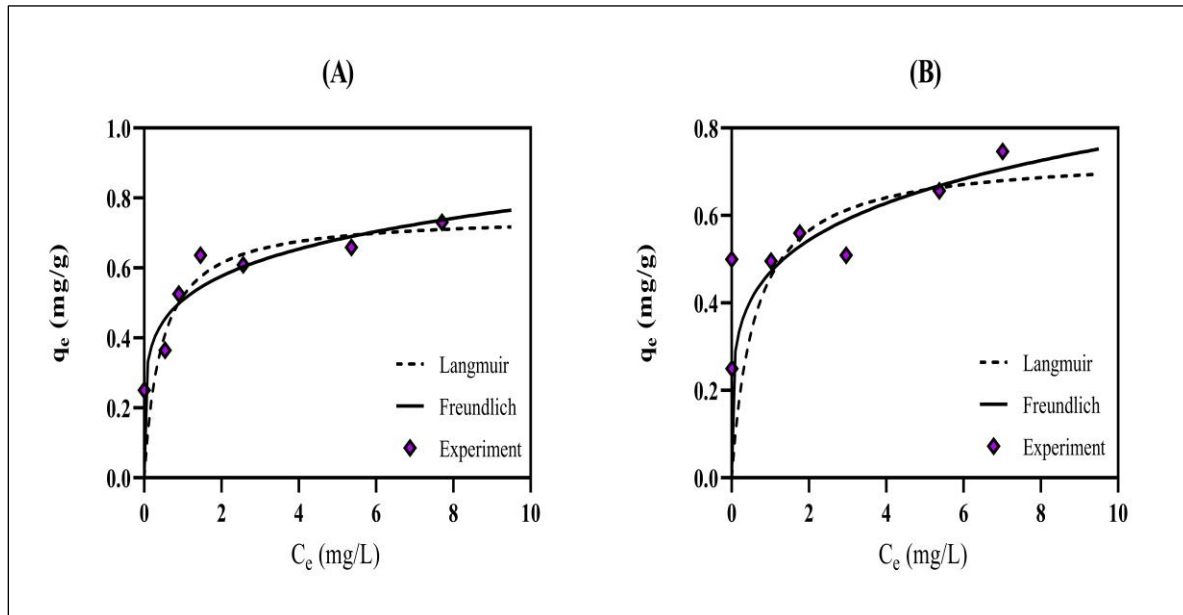


Figure 36. (A-B) Adsorption data and fitted isotherm models for copper with 200 mg aged TP in 50 mL solution

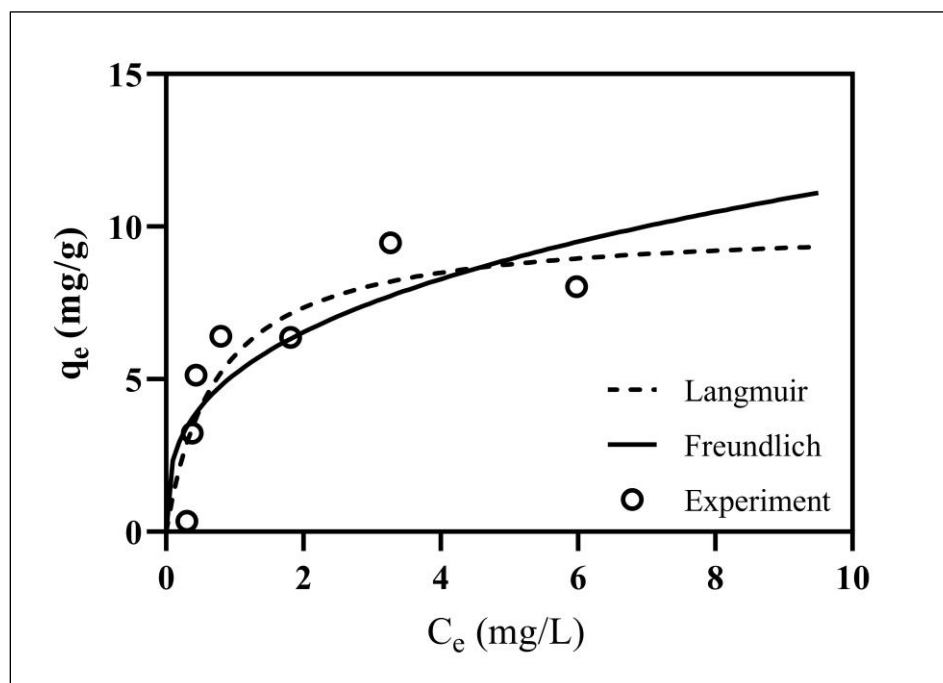


Figure 37. Adsorption data and fitted isotherm models for lead with 100 mg untreated TP in 50 mL solution.

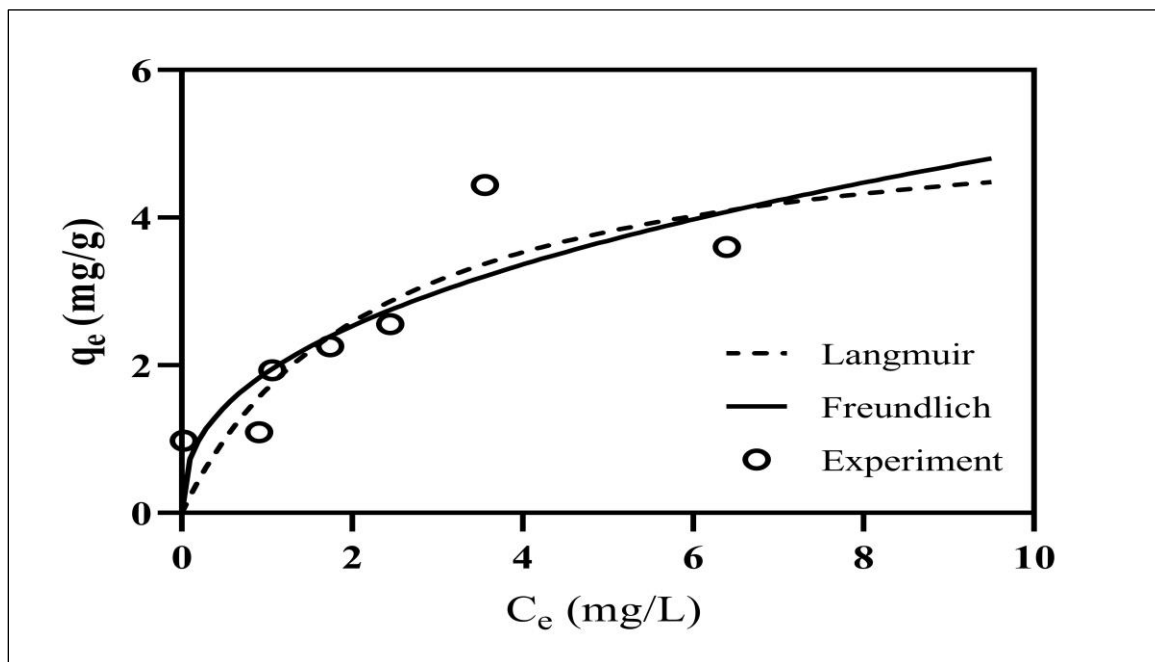


Figure 38. Adsorption data and fitted isotherm models for lead with 50 mg untreated TP in 50 mL solution.

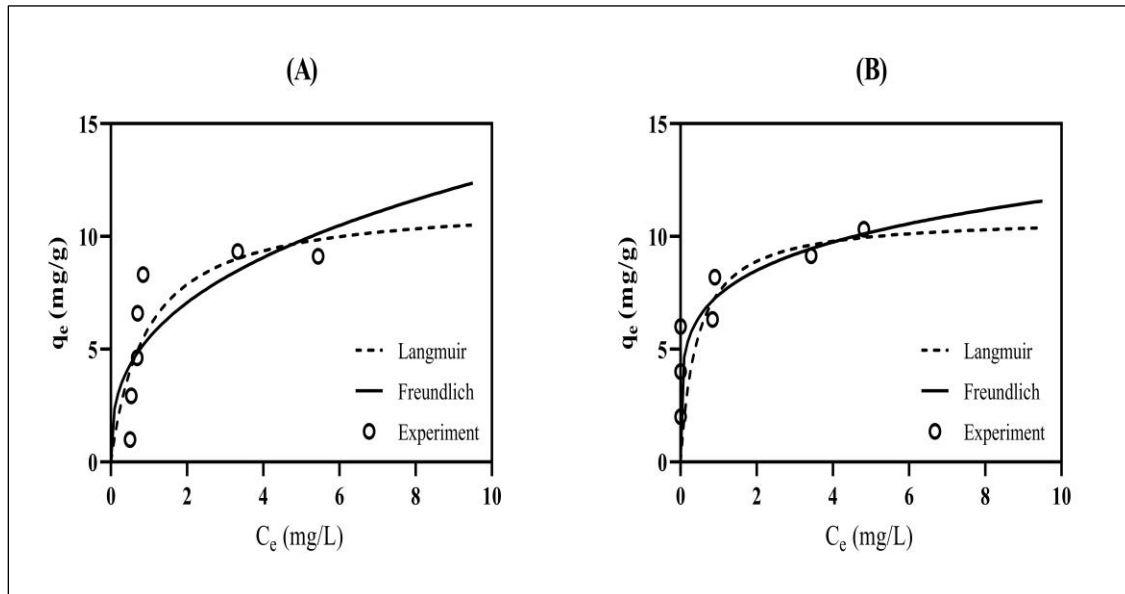


Figure 39.(A-B) Adsorption data and fitted isotherm models for lead with 25 mg untreated TP in 50 mL solution.

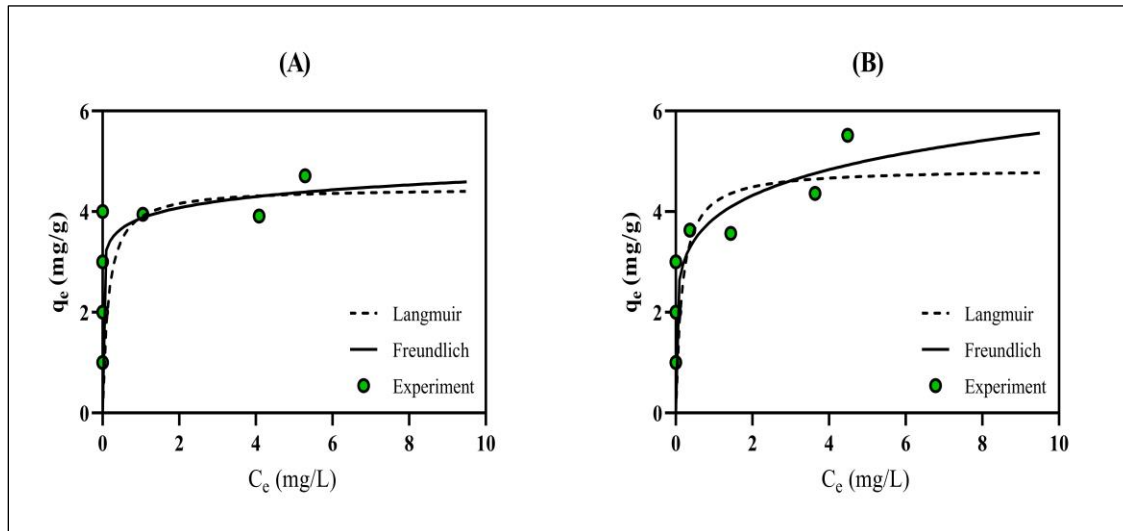


Figure 40. (A-B) Adsorption data and fitted isotherm models for lead with 50 mg aged TP in 50 mL solution.

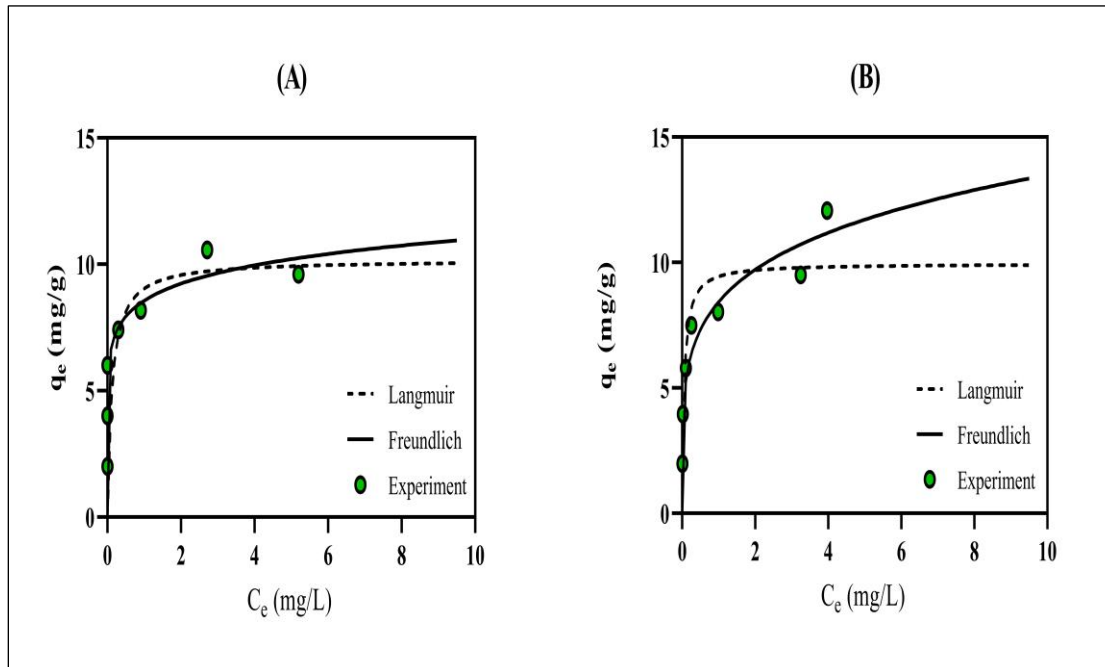


Figure 41. (A-B) Adsorption data and fitted isotherm models for lead with 25 mg aged TP in 50 mL solution.

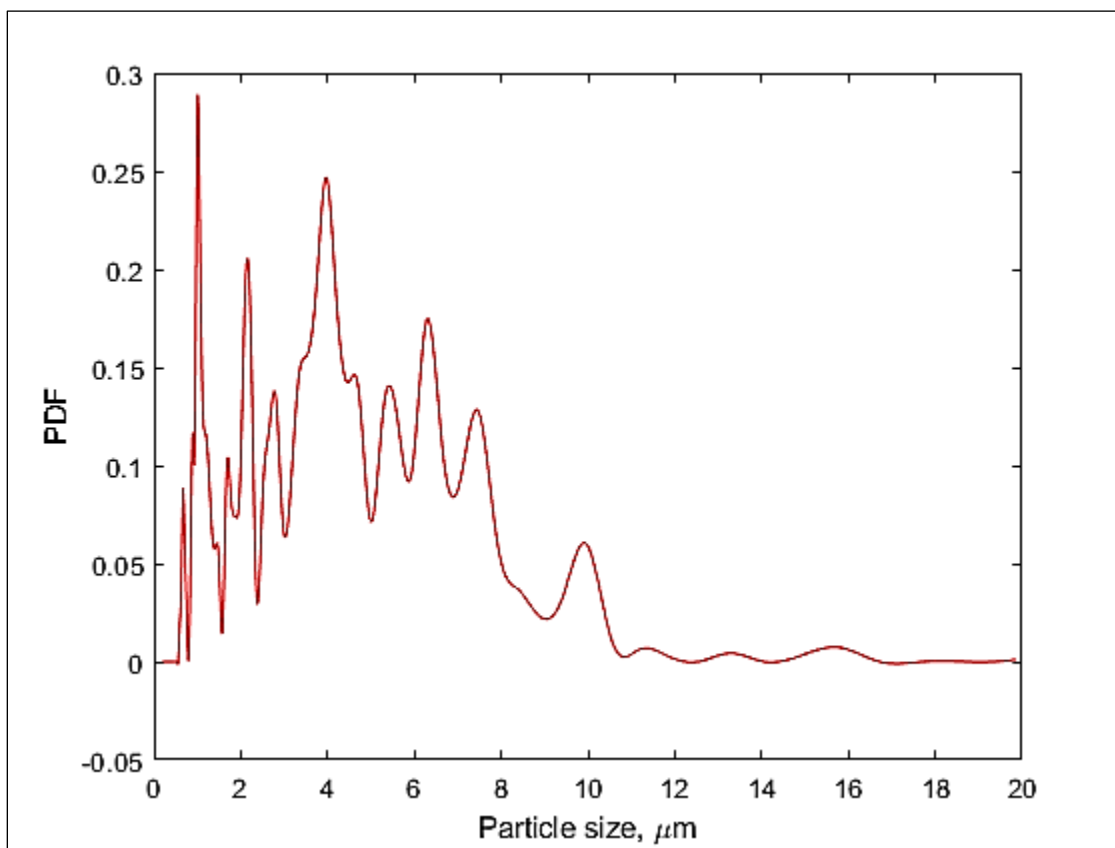
Appendix C: Size Distribution of the Finer Portion of the Aged TP.

Figure 42. Particle size distribution of the finer portion of the aged TP measured by an optical microscope.



OHIO
UNIVERSITY

Thesis and Dissertation Services